



30 1. Introduction

31 New particle formation (NPF), an important source of particles in the atmosphere, is a dynamic
32 process involving interactions among precursor gas molecules, small clusters, and pre-existing
33 particles (Yu and Turco, 2001; Zhang et al., 2012). H_2SO_4 and H_2O are known to play an important
34 role in atmospheric particle formation (e.g., Doyle, 1961). In typical atmospheric conditions, the
35 specie dominating the formation and growth of small clusters is H_2SO_4 . The contribution of H_2O
36 to the nucleation is related to the hydration of H_2SO_4 clusters (or, in the other words, modification
37 of the composition of nucleating clusters) that reduces the H_2SO_4 vapor pressure and hence
38 diminishes the evaporation of H_2SO_4 from the pre-nucleation clusters. NH_3 , the most abundant
39 gas-phase base molecule in the atmosphere and a very efficient neutralizer of sulfuric acid
40 solutions, has long been proposed to enhance nucleation in the lower troposphere (Coffman and
41 Hegg, 1995) although it has been well recognized that earlier versions of classical ternary
42 nucleation model (Coffman and Hegg, 1995; Korhonen et al., 1999; Napari et al., 2002)
43 significantly over-predict the effect of ammonia (Yu, 2006a; Merikanto et al., 2007; Zhang et al.,
44 2010).

45 The impacts of NH_3 on NPF have been investigated in a number of laboratory studies (Kim et
46 al., 1998; Ball et al., 1999; Hanson and Eisele, 2002; Benson et al., 2009; Kirkby et al., 2011;
47 Zollner et al., 2012; Froyd and Lovejoy, 2012; Glasoe et al., 2015; Schobesberger et al., 2015;
48 Kurten et al., 2016) including those recently conducted at the European Organization for Nuclear
49 Research (CERN) in the framework of the CLOUD (Cosmics Leaving OUtdoor Droplets)
50 experiment that has provided a unique dataset for quantitatively examining the dependences of
51 ternary H_2SO_4 - H_2O - NH_3 nucleation rates on concentrations of NH_3 ($[\text{NH}_3]$) and H_2SO_4
52 ($[\text{H}_2\text{SO}_4]$), ionization rate (Q), temperature (T), and relative humidity (RH) (Kirkby et al., 2011;
53 Kurten et al., 2016). The experimental conditions in the CLOUD chamber, a 26.1 m^3 stainless steel
54 cylinder, were well controlled, while impacts of potential contaminants were minimized
55 (Schnitzhofer et al., 2014; Duplissy et al., 2016). Based on CLOUD measurements in H_2SO_4 - H_2O -
56 NH_3 vapor mixtures, Kirkby et al. (2011) reported that an increase of $[\text{NH}_3]$ from ~ 0.03 ppb (parts
57 per billion, by volume) to ~ 0.2 ppb can enhance ion-mediated (or induced) nucleation rate by 2-3
58 orders of magnitude and that the ion-mediated nucleation rate is a factor of 2 to >10 higher than
59 that of neutral nucleation under typical level of contamination by amines. In the presence of
60 ionization, highly polar common atmospheric nucleation precursors such as H_2SO_4 , H_2O , and NH_3
61 molecules tend to cluster around ions; and charged clusters are generally much more stable than
62 their neutral counterparts with enhanced growth rates as a result of dipole-charge interactions (Yu
63 and Turco, 2001).

64 Despite of various laboratory measurements indicate that ammonia enhances NPF, the physio-
65 chemical processes underlying the observed different effects of ammonia on the formation of



66 neutral, positively charged and negatively charged clusters (Schobesberger et al., 2015) are yet to
67 be understood. To achieve such an understanding, nucleation model based on the first principles
68 is needed. Such a model is also necessary to extrapolate data obtained in a limited number of
69 experimental conditions to a wide range of atmospheric conditions, where $[\text{NH}_3]$, $[\text{H}_2\text{SO}_4]$,
70 ionization rates, T, RH and surface areas of preexisting particles vary widely depending on the
71 region, pollution level and season. The present work aims to address these issues by developing a
72 kinetically-based $\text{H}_2\text{SO}_4\text{-H}_2\text{O-NH}_3$ ternary ion-mediated nucleation (TIMN) model that is based
73 on the molecular clustering thermodynamic data. The model predictions are compared with
74 relevant CLOUD measurements and previous studies.

75

76 **2. Kinetic-based $\text{H}_2\text{SO}_4\text{-H}_2\text{O-NH}_3$ ternary ion-mediated nucleation (TIMN) model**

77 2.1. Background

78 Most nucleation models developed in the past for $\text{H}_2\text{SO}_4\text{-H}_2\text{O}$ binary homogeneous nucleation
79 (e.g., Vehkamäki et al., 2002), $\text{H}_2\text{SO}_4\text{-H}_2\text{O}$ ion-induced nucleation (e.g., Hamill et al., 1982; Raes
80 et al., 1986; Laakso et al., 2003), and $\text{H}_2\text{SO}_4\text{-H}_2\text{O-NH}_3$ ternary homogeneous nucleation (Coffman
81 and Hegg, 1995; Korhonen et al., 1999; Napari et al., 2002) have been based on the classical
82 approach, which employs capillarity approximation (i.e., assuming that small clusters have same
83 properties as bulk) and calculate nucleation rates according to the free energy change associated
84 with the formation of a “critical embryo”. Yu and Turco (1997, 2000, 2001) developed a neutral
85 and charged binary $\text{H}_2\text{SO}_4\text{-H}_2\text{O}$ nucleation model using a kinetic approach that explicitly treats
86 the complex interactions among small air ions, neutral and charged clusters of various sizes,
87 precursor vapor molecules, and pre-existing aerosols. The formation and evolution of cluster size
88 distributions for positively and negatively charged cluster ions and neutral clusters affected by
89 ionization, recombination, neutralization, condensation, evaporation, coagulation, and scavenging,
90 has been named as ion-mediated nucleation (IMN) (Yu and Turco, 2000). The IMN theory
91 significantly differs from classical ion-induced nucleation (IIN) theory (e.g., Hamill et al., 1982;
92 Raes et al., 1986; Laakso et al., 2003) which is based on a simple modification of the free energy
93 for the formation of a “critical embryo” by including the electrostatic potential energy induced by
94 the embedded charge (i.e., Thomson effect (Thomson, 1888)). The classical approach does not
95 properly account for the kinetic limitation to embryo development, enhanced stability and growth
96 of charged clusters associated with dipole-charge interaction (Nadykto and Yu, 2003; Yu, 2005),
97 and the important contribution of neutral clusters resulting from ion-ion recombination to
98 nucleation (Yu and Turco, 2011). In contrast, these important physical processes are explicitly
99 considered in the kinetic-based IMN model (Yu, 2006b).

100 Since the beginning of the century, nucleation models based on kinetic approach have also
101 been developed in a number of research groups (Lovejoy et al., 2004; Sorokin et al., 2006; Chen



102 et al., 2012; Dawson et al., 2012; McGrath et al., 2012). Lovejoy et al. (2004) developed a kinetic
103 ion nucleation model, which explicitly treats the evaporation of small neutral and negatively
104 charged $\text{H}_2\text{SO}_4\text{-H}_2\text{O}$ clusters. The thermodynamic data used in their model were obtained from
105 measurements of small ion clusters, ab initio calculations, thermodynamic cycle, and some
106 approximations (adjustment of Gibbs free energy for neutral clusters calculated based on liquid
107 droplet model, interpolation, etc.). Lovejoy et al. (2004) didn't consider the nucleation on positive
108 ions. Sorokin et al. (2006) developed an ion-cluster-aerosol kinetic (ICAK) model which uses the
109 thermodynamic data reported in Froyd and Lovejoy (2003a, b) and empirical correction terms
110 proposed by Lovejoy et al. (2004). Sorokin et al. (2006) used the ICAK model to simulate
111 dynamics of neutral and charged $\text{H}_2\text{SO}_4\text{-H}_2\text{O}$ cluster formation and compared the modeling results
112 with their laboratory measurements. Chen et al. (2012) developed an approach for modeling new
113 particle formation based on a sequence of acid-base reactions, with sulfuric acid evaporation rates
114 (from clusters) estimated empirically based on measurements of neutral molecular clusters taken
115 in Mexico City and Atlanta. Dawson et al. (2012) presented a semi-empirical kinetics model for
116 nucleation of methanesulfonic acid (MSA), amines, and water that explicitly accounted for the
117 sequence of reactions leading to formation of stable particles. The kinetic models of Chen et al.
118 (2012) and Dawson et al. (2012) consider only neutral clusters.

119 McGrath et al. (2012) developed the Atmospheric Cluster Dynamics Code (ACDC) to model
120 the cluster kinetics by solving the birth–death equations explicitly, with evaporation rate
121 coefficients derived from formation free energies calculated by quantum chemical methods.
122 ACDC is also an acid–base reaction model, with the largest clusters containing 4–5 acid and 4–5
123 base molecules (no water molecules) (Almeida et al., 2013; Olenius et al., 2013). The ACDC
124 model applied to the $\text{H}_2\text{SO}_4\text{-dimethylamine}$ (DMA) system considers 0–4 base molecules and 0–
125 4 sulfuric acid molecules (Almeida et al., 2013). Olenius et al. (2013) applied the ACDC model to
126 simulate the steady-state concentrations and kinetics of neutral, and negatively and positively
127 charged clusters containing up to 5 H_2SO_4 and 5 NH_3 molecules. In ACDC, the nucleation rate is
128 calculated as the rate of clusters growing larger than the upper bounds of the simulated system
129 (i.e., clusters containing 4 or 5 H_2SO_4 molecules) (Kurten et al., 2016) and thus may over-predict
130 nucleation rates when critical clusters contain more than 5 H_2SO_4 molecules. All clusters simulated
131 by the ACDC model do not contain H_2O molecules and the effect of relative humidity (RH) on
132 nucleation thermochemistry is neglected.

133 The kinetic IMN model developed by Yu and Turco (1997, 2001) explicitly simulates the
134 dynamics of neutral, positively charged, and negatively charged clusters, based on a discrete-
135 sectional bin structure that covers the clusters containing 0, 1, 2, ..., 15, ... H_2SO_4 molecules to
136 particles containing thousands of H_2SO_4 (and H_2O) molecules. In the first version of the kinetic
137 IMN model (Yu and Turco, 1997, 2001), due to the lack of thermodynamic data for the small



138 clusters, the compositions of neutral and charged clusters were assumed to be the same and the
139 evaporation of small clusters was accounted for using a simple adjustment to the condensation
140 accommodation coefficients. Yu (2006b) developed a second-generation IMN model which
141 incorporated newer thermodynamic data (Froyd, 2002; Wilhelm et al., 2004) and physical
142 algorithms (Froyd, 2002; Wilhelm et al., 2004) and explicitly treated the evaporation of neutral
143 and charged clusters. Yu (2007) further improved the IMN model by using two independent
144 measurements (Marti et al., 1997; Hanson and Eisele, 2000) to constrain monomer hydration in
145 the H₂SO₄-H₂O system and by incorporating experimentally determined energetics of small
146 neutral H₂SO₄-H₂O clusters that became available then (Hanson and Lovejoy, 2006; Kazil et al.,
147 2007). The first and second generations of the IMN model were developed for the H₂SO₄-H₂O
148 binary system, although the possible effects of ternary species such as the impact of NH₃ on the
149 stability of both neutral and charged pre-nucleation clusters have been pointed out in these
150 previous studies (Yu and Turco, 2001; Yu, 2006b). The present work extends the previous versions
151 of the IMN model in binary H₂SO₄-H₂O system to ternary H₂SO₄-H₂O-NH₃ system, as described
152 below. The thermodynamic data sets used for binary clusters were also updated.

153

154 2.2. Model representation of kinetic ternary nucleation processes

155 Figure 1 schematically illustrates the evolution of charged and neutral clusters/droplets
156 explicitly simulated in the kinetic H₂SO₄-H₂O-NH₃ TIMN model. Here, H₂SO₄ (S) is the key
157 atmospheric nucleation precursor driving the TIMN process while ions, H₂O (W), and NH₃ (A)
158 stabilize the H₂SO₄ clusters and enhance in this way H₂SO₄ nucleation rates. Ions also enhance
159 cluster formation rates due to the interaction with polar nucleating species leading to enhanced
160 collision cross sections (Nadykto and Yu, 2003). The airborne ions are generated by galactic
161 cosmic rays (GCRs) or produced by radioactive emanations, lightning, corona discharge,
162 combustion and other ionization sources. The initial negative ions, which are normally assumed to
163 be NO₃⁻, are converted into HSO₄⁻ core ions (i.e., S⁻) and, then, to larger H₂SO₄ clusters in the
164 presence of gaseous H₂SO₄. The initial positive ions H⁺W_w are converted into H⁺A₁₋₂W_w in the
165 presence of NH₃, H⁺S_sW_w in the presence of H₂SO₄, or H⁺A_aS_sW_w in the case, when both NH₃
166 and H₂SO₄ are present in the nucleating vapors. Some of the binary H₂SO₄-H₂O clusters, both
167 neutral and charged, transform into ternary ones by taking up NH₃ vapors. The molar fraction of
168 ternary clusters in nucleating vapors depends on [NH₃], the binding strength of NH₃ to binary and
169 ternary pre-nucleation clusters, cluster composition, and ambient conditions such as T and RH.



170 Similar to the kinetic binary IMN (BIMN) model (Yu, 2006b), the kinetic TIMN model
 171 employs a discrete-sectional bin structure to represent clusters/particles. The bin index i represent
 172 the amount of core component (i.e., H_2SO_4). For small clusters ($i \leq i_d = 30$ in this study), i is the
 173 number of H_2SO_4 molecules in the cluster (i.e., $i = s$) and the core volume of i^{th} bin $v_i = i \times v_l$, where
 174 v_l is the volume of one H_2SO_4 molecule. When $i > i_d$, $v_i = \text{VRAT}_i \times v_{i-1}$, where VRAT_i is the volume
 175 ratio of i^{th} bin to $(i-1)^{\text{th}}$ bin. The discrete-sectional bin structure enables the model to cover a wide
 176 range of sizes of nucleating clusters/particles with the highest possible size resolution for small
 177 clusters (Yu, 2006b). For clusters with a given bin i , the associated amounts of water and NH_3 and
 178 thus the effective radius of each ternary cluster are calculated based on the equilibrium of
 179 clusters/particles with the water vapor and/or ammonia, as described in later sections.

180 The evolution of positive, negative, and neutral clusters due to the simultaneous condensation,
 181 evaporation, recombination, coagulation, and other loss processes, is described by the following
 182 differential equations obtained by the modification of those describing for the evolution of binary
 183 H_2SO_4 - H_2O system (Yu, 2006b):

$$184 \quad \frac{\partial N_0^+}{\partial t} = Q + \gamma_1^+ N_1^+ - N_0^+ \left(\sum_{j=1}^{i_{\max}} \beta_{i,j}^+ N_j^0 + \sum_{j=0}^{i_{\max}} \eta_{i,j}^+ N_j^+ + \sum_{j=0}^{i_{\max}} \alpha_{0,j}^{+,-} N_j^- \right) - N_0^+ L_0^+ \quad (1)$$

$$185 \quad \frac{\partial N_0^-}{\partial t} = Q + \gamma_1^- N_1^- - N_0^- \left(\sum_{j=1}^{i_{\max}} \beta_{i,j}^- N_j^0 + \sum_{j=0}^{i_{\max}} \eta_{i,j}^- N_j^- + \sum_{j=0}^{i_{\max}} \alpha_{0,j}^{-,+} N_j^+ \right) - N_0^- L_0^- \quad (2)$$

$$186 \quad \frac{\partial N_1^0}{\partial t} = P_{\text{H}_2\text{SO}_4} + \sum_{j=2}^{i_{\max}} \delta_{j,2} \gamma_j^0 N_j^0 + \sum_{j=1}^{i_{\max}} (\gamma_j^+ N_j^+ + \gamma_j^- N_j^-) - N_1^0 \left(\sum_{j=1}^{i_{\max}} (1 - f_{1,j,1}) \beta_{1,j}^0 N_j^0 + \sum_{j=0}^{i_{\max}} (\beta_{j,1}^+ N_j^+ + \beta_{j,1}^- N_j^-) \right) - N_1^0 L_1^0 \quad (3)$$

$$187 \quad \frac{\partial N_i^+(i \geq 1)}{\partial t} = g_{i+1,i} \gamma_{i+1}^+ N_{i+1}^+ - g_{i,i-1} \gamma_i^+ N_i^+ + \sum_{j=0}^{i-1} \sum_{k=1}^i \frac{v_j}{v_i} f_{j,k,i} \beta_{j,k}^+ N_j^+ N_k^0 + \sum_{j=0}^{i-1} \sum_{k=0}^i \frac{v_j}{v_i} f_{j,k,i} \eta_{j,k}^+ N_j^+ N_k^+ + \sum_{j=0}^i \sum_{k=1}^i \frac{v_k}{v_i} f_{j,k,i} \beta_{j,k}^+ N_j^+ N_k^0 - N_i^+ \left(\sum_{j=1}^{i_{\max}} (1 - f_{i,j,i}) \beta_{i,j}^+ N_j^0 + \sum_{j=0}^{i_{\max}} (1 - f_{i,j,i}) \eta_{i,j}^+ N_j^+ + \sum_{j=0}^{i_{\max}} \alpha_{i,j}^{+,-} N_j^- \right) - N_i^+ L_i^+ \quad (4)$$

$$188 \quad \frac{\partial N_i^-(i \geq 1)}{\partial t} = g_{i+1,i} \gamma_{i+1}^- N_{i+1}^- - g_{i,i-1} \gamma_i^- N_i^- + \sum_{j=0}^{i-1} \sum_{k=1}^i \frac{v_j}{v_i} f_{j,k,i} \beta_{j,k}^- N_j^- N_k^0 + \sum_{j=0}^{i-1} \sum_{k=0}^i \frac{v_j}{v_i} f_{j,k,i} \eta_{j,k}^- N_j^- N_k^- + \sum_{j=0}^i \sum_{k=1}^i \frac{v_k}{v_i} f_{j,k,i} \beta_{j,k}^- N_j^- N_k^0 - N_i^- \left(\sum_{j=1}^{i_{\max}} (1 - f_{i,j,i}) \beta_{i,j}^- N_j^0 + \sum_{j=0}^{i_{\max}} (1 - f_{i,j,i}) \eta_{i,j}^- N_j^- + \sum_{j=0}^{i_{\max}} \alpha_{i,j}^{-,+} N_j^+ \right) - N_i^- L_i^- \quad (5)$$



$$\begin{aligned}
 189 \quad \frac{\partial N_i^0(i \geq 2)}{\partial t} &= g_{i+1,i} \gamma_{i+1}^0 N_{i+1}^0 - g_{i,i-1} \gamma_i^0 N_i^0 + \sum_{j=k=1}^i \sum_{v_i}^{i-1} \frac{v_k}{v_i} f_{j,k,i} \beta_{j,k}^0 N_j^0 N_k^0 \\
 &+ \sum_{j=0}^i \sum_{k=0}^i f_{j,k,i} \alpha_{j,k}^{+,-} \left(\frac{v_k}{v_i} N_j^+ N_k^- + \frac{v_j}{v_i} N_j^- N_k^+ \right) - N_i^0 \left(\sum_{j=1}^{i_{\max}} (1 - f_{i,j,i}) \beta_{i,j}^0 N_j^0 + \sum_{j=0}^{i_{\max}} (\beta_{j,i}^+ N_j^+ + \beta_{j,i}^- N_j^-) \right) - N_i^0 L_i^0
 \end{aligned} \quad (6)$$

190

191 In Eqs. (1-6), the superscripts “+”, “-”, and “0” refer to positive, negative, and neutral clusters,

192 respectively, while subscripts i, j, k represent the bin indexes. $N_0^{+,-}$ and Q are the concentration of193 initial ions not containing H_2SO_4 and the ionization rate, respectively. N_i is the total number194 concentration (cm^{-3}) of all cluster/particles (binary + ternary) in the bin i . For small clusters ($i \leq i_d$),195 N_i is the number concentration (cm^{-3}) of all clusters containing i H_2SO_4 molecules. For example,196 N_1^0 is the total concentration of binary and ternary neutral clusters containing one H_2SO_4 197 molecules. $P_{\text{H}_2\text{SO}_4}$ is the production rate of neutral H_2SO_4 molecules. $L_i^{+,-,0}$ is the loss rate due to

198 scavenging by pre-existing particles, and wall and dilution losses in the laboratory chamber studies

199 (Kirkby et al., 2011; Olenius et al., 2013; Kurten et al., 2016). $f_{j,k,i}$ is the volume fraction of200 intermediate particles (volume = $v_j + v_k$) partitioned into bin i with respect to the core component201 – H_2SO_4 , as defined in Jacobson et al. (1994). $g_{i+1,i} = v_1 / (v_{i+1} - v_i)$ is the volume fraction of202 intermediate particles of volume ($v_{i+1} - v_1$) partitioned into bin i . $\delta_{j,2} = 2$ at $j=2$ and $\delta_{j,2} = 1$ at $j \neq 2$.203 γ_i^+ , γ_i^- , and γ_i^0 are the mean (or effective) cluster evaporation coefficients for positive, negative204 and neutral clusters in bin i , respectively. $\beta_{i,j}^+$, $\beta_{i,j}^-$, $\beta_{i,j}^0$ are the coagulation kernels for the205 neutral clusters/particles in bin j interacting with positive, negative, and neutral clusters/particles206 in bin i , respectively, which reduce to the condensation coefficients for H_2SO_4 monomers at $j=1$.207 $\eta_{j,k}^+$ and $\eta_{j,k}^-$ are coagulation kernels for clusters/particles of like sign from bin j and208 clusters/particles from bin k . $\alpha_{i,j}^{+,-}$ is the recombination coefficient for positive clusters/particles209 in bin i interacting with negative clusters/particles in bin j , while $\alpha_{i,j}^{-,+}$ is the recombination



210 coefficient negative clusters/particles from bin i interacting with positively charged
211 clusters/particles from bin j .

212 The methods for calculating β , γ , η , and α for binary H_2SO_4 - H_2O clusters have been described
213 in detail in Yu (2006b). Since β , η , and α depend on the cluster mass (or size) rather than on the
214 cluster composition, schemes for calculating these properties in binary and ternary clusters are
215 identical (Yu, 2006b). In contrast, γ is quite sensitive to cluster composition. The evaporation rate

216 coefficient of H_2SO_4 molecules from clusters containing i H_2SO_4 molecules (γ_i) is largely

217 controlled by the stepwise Gibbs free energy change $\Delta G_{i-1,i}$ of formation of an i -mer from an (i -

218 1)-mer (Yu, 2007)

$$219 \quad \gamma_i = \beta_{i-1} N^0 \exp\left(\frac{\Delta G_{i-1,i}}{RT}\right) \quad (7)$$

$$220 \quad \Delta G_{k-1,k} = \Delta H_{k-1,k}^0 - T\Delta S_{k-1,k}^0 \quad (8)$$

221 where R is the molar gas constant, N^0 is the number concentration of H_2SO_4 at a given T under the
222 reference vapor pressure P of 1 atm. ΔH^0 and ΔS^0 are enthalpy and entropy changes under the

223 standard conditions ($T=298$ K, $P=1$ atm), respectively. The temperature dependence of ΔH^0 and

224 ΔS^0 , which is generally small and typically negligible over the temperature range of interest, was

225 not considered.

226 ΔH , ΔS and ΔG values needed to calculate cluster evaporation rates for the TIMN model can
227 be derived from laboratory measurements and computational quantum chemistry (QC) calculation.
228 Thermochemical properties of neutral and charged binary and ternary clusters obtained using the
229 computational chemical methods and comparisons of computed energies with available
230 experimental data and semi-experimental estimates are given below.

231

232 2.3. Quantum-chemical studies of neutral and charged binary and ternary clusters

233 Thermochemical data for small neutral and charged binary H_2SO_4 - H_2O and ternary H_2SO_4 -
234 H_2O - NH_3 clusters has been reported in a number of earlier publications (Bandy and Ianni, 1998;
235 Ianni and Bandy, 1999; Torpo et al., 2007; Nadykto et al., 2008; Herb et al., 2011, 2013; Temelso
236 et al., 2012a, b; DePalma et al., 2012; Ortega et al., 2012; Chon et al., 2014; Husar et al., 2014;
237 Henschel et al., 2014, 2016; Kurten et al., 2015). The PW91PW91/6-311++G(3df,3pd) method,



238 which is a combination of the Perdue-Wang PW91PW91 density functional with the largest Pople
239 6-311++G(3df,3pd) basis set, has thoroughly been validated and agrees well with existing
240 experimental data. In earlier studies, this method has been applied to a large variety of
241 atmospherically-relevant clusters (Nadykto et al. 2006, 2007a, b, 2008, 2014, 2015; Torpo et al.
242 2007; Zhang et al., 2009; Elm et al. 2012; Leverentz et al. 2013; Xu and Zhang, 2012; Xu and
243 Zhang, 2013; Elm et al., 2013; Zhu et al. 2014; Bork et al. 2014; Elm and Mikkelsen, 2014; Peng
244 et al. 2015; Miao et al 2015; Chen et al., 2015; Ma et al., 2016) and has been shown to be well
245 suited to study the ones, as evidenced by a very good agreement of the computed values with
246 measured cluster geometries, vibrational fundamentals, dipole properties and formation Gibbs free
247 energies (Nadykto et al., 2007a, b, 2008, 2014, 2015; Herb et al., 2013; Elm et al., 2012, 2013;
248 Leverentz et al., 2013; Bork et al., 2014) and with high level ab initio results (Temelso et al., 2012a,
249 b; Husar et al., 2012; Bustos et al., 2014).

250 We have extended the earlier QC studies of binary and ternary clusters to larger sizes. The
251 computations have been carried out using Gaussian 09 suite of programs (Frisch et al., 2009). In
252 order to ensure the quality of the conformational search we have carried out a thorough sampling
253 of conformers. We have used both basin hopping algorithm, as implemented in Biovia Materials
254 Studio 8.0, and locally developed sampling code, which creates a “mesh” around the cluster, in
255 which molecules being attached to the cluster are the mesh nodes. Typically, for each cluster of a
256 given chemical composition a thousand to several thousands of isomers have been sampled. We
257 used a three-step optimization procedure, which includes (i) pre-optimization of initial/guess
258 geometries by semi-empirical PM6 method, separation of the most stable isomers located within
259 15 kcal mol⁻¹ of the intermediate global minimum and duplicate removal, followed by (ii)
260 optimization of the selected isomers meeting the aforementioned stability criterion by
261 PW91PW91/CBSB7 method and (iii) the final optimization of the most stable at
262 PW91PW91/CBSB7 level isomers within 5 kcal mol⁻¹ of the current global minimum using
263 PW91PW91/6-311++G(3df,3pd) method. Typically, only ~4-30% of initially sampled isomers
264 reach the second (PW91PW91/CBSB7) level, where ~10-40% of isomers optimized with
265 PW91PW91/CBSB7 are selected for the final run. Typically, the number of equilibrium isomers
266 of hydrated clusters is larger than that of unhydrated ones of similar chemical composition. Table
267 1 shows the numbers of isomers converged at the final PW91PW91/6-311++G(3df,3pd)
268 optimization step for selected clusters and HSG values of the most stable isomers used in the
269 present study. The number of isomers optimized at the PW91PW91/6-311++G(3df,3pd) level of
270 theory varies from case to case, typically being in the range of ~10-200.

271 The computed stepwise enthalpy, entropy, and Gibbs free energies of cluster formation have
272 been thoroughly evaluated and used to calculate the evaporation rates of H₂SO₄ from neutral,



273 positive and negative charged clusters. A detailed description of QC calculations and the full range
274 of computed properties of binary and ternary clusters will be reported in separate papers.

275

276 2.3.1 Positively charged clusters

277 Table 2 presents the computed stepwise Gibbs free energy changes under standard conditions
278 (ΔG^0) for positive binary and ternary clusters, along with the corresponding experimental data or
279 semi-experimental estimates. Figure 2 shows ΔG associated with the addition of water (ΔG_{+W}^0),
280 ammonia (ΔG_{+A}^0), and sulfuric acid (ΔG_{+S}^0) to binary and ternary clusters as a function of the cluster
281 hydration number w .

282 H_2O has high proton affinity and, thus, H_2O is strongly bonded to all positive ions with low w .
283 ΔG_{+W}^0 expectedly becomes less negative and binding of H_2O to binary and ternary clusters
284 weakens due to the screening effect as the hydration number w is growing (Fig. 2a). The presence
285 of NH_3 in the clusters weakens binding of H_2O to positive ions. For example, ΔG_{+W}^0 for
286 $H^+A_1W_wS_1$ is ~ 3 -4 kcal mol $^{-1}$ less negative than that for $H^+W_wS_1$ at $w=3$ -6. The addition of one
287 more NH_3 to the clusters to form $H^+A_2W_w$ and $H^+A_2W_wS_1$ further weakens H_2O binding by ~ 1.5 -
288 6 kcal mol $^{-1}$ at $w=1$ -3, while exhibiting much smaller impact on hydration free energies at $w>3$.
289 Both the absolute values and trends in ΔG_{+W}^0 derived from calculations are in agreement with the
290 laboratory measurements within the uncertainty range of ~ 1 -2 kcal mol $^{-1}$ for both QC calculations
291 and measurements. This confirms the efficiency and precision of QC methods in calculating
292 thermodynamic data needed for the development of nucleation models.

293 The proton affinity of NH_3 is 204.1 kcal mol $^{-1}$, which is 37.5 kcal mol $^{-1}$ higher than that of
294 H_2O (166.6 kcal mol $^{-1}$) (Jolly, 1991). The hydrated hydronium ions (H^+W_w) are easily converted
295 to $H^+A_1W_w$ in the presence of NH_3 . The binding of NH_3 and H_2O molecule to H^+W_w exhibits
296 similar pattern. In particular, binding of NH_3 to H^+W_w decreases as w is growing, with ΔG_{+A}^0 for
297 $H^+A_1W_w$ ranging from -52.08 kcal mol $^{-1}$ at $w=1$ to -8.32 kcal mol $^{-1}$ at $w=9$. The binding of NH_3
298 to $H^+W_wS_1$ ions is also quite strong, with ΔG_{+A}^0 for $H^+A_1W_wS_1$ ranging from -33.14 kcal mol $^{-1}$ at
299 $w=1$ and to -10.57 kcal mol $^{-1}$ at $w=6$. The addition of the NH_3 molecule to $H^+A_1W_w$ (to form
300 $H^+A_2W_w$) is much less favorable thermodynamically than that to H^+W_w , with the corresponding
301 ΔG_{+A}^0 being -22 kcal mol $^{-1}$ and -6 kcal mol $^{-1}$ at $w=2$ and $w=6$, respectively. The ΔG_{+A}^0 values for
302 $H^+A_2W_w$ are 3-5 kcal mol $^{-1}$ more negative than the experimental values at $w=0$ -1; however, they
303 are pretty close to experimental data at $w=2$ -3 (Fig. 2b and Table 2). While it is possible that the
304 QC method overestimates the charge effect on the formation free energies of smallest clusters, the
305 possible overestimation at $w=0$ -1 will not affect nucleation calculations because most of $H^+A_2W_w$
306 in the atmosphere contain more than 2 water molecules (i.e., $w>2$) due to the strong hydration (see
307 Table 2 and Fig. 2a).



308 A comparison of QC and semi-experimental estimates of ΔG_{+S}^0 values associated with the
309 attachment of H_2SO_4 to positive ions shown in Fig. 2c indicates that computed ΔG_{+S}^0 values agree
310 well with observations for $\text{H}^+\text{W}_w\text{S}_1$ and $\text{H}^+\text{A}_1\text{W}_w\text{S}_1$ but differ by $\sim 2\text{--}4$ kcal mol $^{-1}$ from semi-
311 experimental values for $\text{H}^+\text{A}_2\text{W}_w\text{S}_1$. As seen from Figs. 2a and 2c, the attachment of NH_3 to
312 $\text{H}^+\text{W}_w\text{S}_1$ weakens the binding of both H_2O and H_2SO_4 to the clusters. This suggests that the
313 attachment of NH_3 leads to the evaporation of H_2SO_4 and H_2O molecules from the clusters. In
314 other words, H_2SO_4 is less stable in $\text{H}^+\text{A}_1\text{W}_w\text{S}_1$ than in $\text{H}^+\text{W}_w\text{S}_1$ (Fig. 2c). While this may be taken
315 for the indication that NH_3 inhibits nucleation on positive ions at the first look, further calculations
316 show that binding of NH_3 to $\text{H}^+\text{A}_1\text{W}_w\text{S}_1$ is quite strong (Fig. 2b) and that H_2SO_4 in $\text{H}^+\text{A}_2\text{W}_w\text{S}_1$
317 cluster is much more stable than that in $\text{H}^+\text{A}_1\text{W}_w\text{S}_1$, with ΔG_{+S}^0 being by ~ 7 kcal mol $^{-1}$ more
318 negative at $w > 2$. The $\text{H}^+\text{A}_2\text{W}_w\text{S}_1$ cluster can also be formed via the attachment of H_2SO_4 to
319 $\text{H}^+\text{A}_2\text{W}_w$. In the presence of sufficient concentrations of NH_3 , a large fraction of positively charged
320 H_2SO_4 monomers exist in the form of $\text{H}^+\text{A}_2\text{W}_w\text{S}_1$ and, hence, NH_3 enhances nucleation of positive
321 ions. Since positively charged H_2SO_4 dimers are expected to contain large number of water
322 molecules, no quantum chemical data for these clusters are available. The CLOUD measurements
323 do indicate that once $\text{H}^+\text{A}_2\text{W}_w\text{S}_1$ are formed, they can continue to grow to larger $\text{H}^+\text{A}_a\text{W}_w\text{S}_s$
324 clusters along $a=s+1$ pathway (Schobesberger et al., 2015).

325 Table 2 and Figure 2 show clearly that the calculated values in most cases agree with
326 measurements within the uncertainty range that justifies the application of QC values in the case,
327 when no reliable experimental data are available.

328

329 2.3.2 Neutral clusters

330 Table 3 presents the computed stepwise Gibbs free energy changes for the formation of ternary
331 $\text{S}_s\text{A}_a\text{W}_w$ clusters under standard conditions. The thermodynamic properties of the S_1A_1 have been
332 reported in a number of computational studies (e.g., Herb et al., 2011; Kurten et al., 2015; Nadykto
333 and Yu, 2007). However, as pointed out by Kurten et al. (2015), most of these studies, except for
334 Nadykto and Yu (2007), did not consider the impact of H_2O on cluster thermodynamics. We have
335 extended the earlier studies of Nadykto and Yu (2007) and Herb et al. (2011) to larger clusters up
336 to S_4A_5 (no hydration) and up to S_2A_2 (hydration included). The free energy of binding of NH_3 to
337 H_2SO_4 (or H_2SO_4 to NH_3) obtained using our method is -7.77 kcal mol $^{-1}$ that is slightly more
338 negative than values reported by other groups (-6.6 – -7.61 kcal mol $^{-1}$) and within less than 0.5 kcal
339 mol $^{-1}$ of the experimental value of -8.2 kcal mol $^{-1}$ derived from CLOUD measurements (Kurten et
340 al., 2015).

341 As it may be seen from Table 3, the NH_3 binding to S_{1-2}W_w weakens as w increases. The
342 average ΔG_{+W}^0 for S_1W_w formation derived from a combination of laboratory measurements and
343 quantum chemical studies are -3.02 , -2.37 , and -1.40 kcal mol $^{-1}$ for the first, second, and third



344 hydration, respectively (Yu, 2007). This indicates that a large fraction of H₂SO₄ monomers in the
345 Earth's atmosphere is likely hydrated. Therefore, the decreasing NH₃ binding strength to hydrated
346 H₂SO₄ monomers implies that RH (and T) will affect the relative abundance of H₂SO₄ monomers
347 containing NH₃. Currently, no experimental data or observations are available to evaluate the
348 impact of hydration (or RH) on ΔG_{+A}^0 . Table 3 shows that the presence of NH₃ in H₂SO₄ clusters
349 suppress hydration and that ΔG_{+W}^0 for S₂A₂ falls below -2.0 kcal mol⁻¹. This is consistent with
350 earlier studies by our group and others showing that large S_nA_n clusters ($n > 2$) are not hydrated
351 under typical atmospheric conditions. In the present study, the hydration of neutral S_nA_n clusters
352 at $n > 2$ is neglected.

353 The number of NH₃ molecules in the cluster (or H₂SO₄ to NH₃ ratio) significantly affects ΔG_{+S}^0
354 and ΔG_{+A}^0 values. For example, ΔG_{+S}^0 for S₃A_a clusters increases from -7.08 kcal mol⁻¹ to -16.92
355 kcal mol⁻¹ and ΔG_{+A}^0 decreases from -16.14 kcal mol⁻¹ to -8.93 kcal mol⁻¹ as a is growing from 1
356 to 3. For S₄A_a clusters, ΔG_{+S}^0 is increasing from -7.48 kcal mol⁻¹ to -16.26 kcal mol⁻¹ and ΔG_{+A}^0
357 decreases from -17.16 kcal mol⁻¹ to -11.34 kcal mol⁻¹ as a increases from 2 to 4. ΔG_{+A}^0 for S₄A₁
358 cluster is by 1.38 kcal mol⁻¹ less negative than that for S₄A₂. ΔG_{+S}^0 for the S₄A₁ cluster is also quite
359 low (-4.16 kcal mol⁻¹) that might indicate the possible existence of a more stable S₄A₁ isomer,
360 which is yet to be identified. In the presence of NH₃, the uncertainty in the thermochemistry data
361 for S₄A₁ will not significantly affect ternary nucleation rates because most of S₄-clusters contain
362 3 or 4 NH₃ molecules.

363 For the S_sA_a clusters with $s=a$, ΔG_{+A}^0 increases as cluster is growing while ΔG_{+S}^0 first increases
364 significantly as S₁A₁ is converting into S₂A₂ and then levels off as S₂A₂ is converting into S₄A₄.
365 We also observe a significant drop in ΔG_{+A}^0 in the case when NH₃/H₂SO₄ ratio exceeds 1. This
366 finding is fully consistent with the laboratory measurements showing that growth of neutral S_sA_a
367 clusters follows $s=a$ pathway (Schobesberger et al., 2015).

368

369 2.3.3 Negative ionic clusters

370 Table 4 shows ΔG_{+W} , ΔG_{+A} , and ΔG_{+S} needed to form negatively charged clusters under
371 standard conditions, along with available semi-experimental values (Froyd and Lovejoy, 2003).
372 H₂O binding to negatively charged S⁻S_s clusters significantly strengthens with increasing s , from
373 $\Delta G_{+W}^0 = -0.61$ to -1.83 kcal mol⁻¹ at $s=1-2$ to $\Delta G_{+W}^0 = -3.5$ kcal mol⁻¹ at $w=1$ and -2.25 kcal mol⁻¹ at
374 $w=4$ at $s=4$. ΔG_{+W}^0 values at $s=3$ and 4 are slightly more negative (by $\sim 0.1 - 0.9$ kcal mol⁻¹) than
375 those reported by Froyd and Lovejoy (2003). Just like H₂O binding, NH₃ binding to S⁻S_s at $s < 3$ is
376 very weak, with ΔG_{+A}^0 ranging from +2.81 kcal mol⁻¹ at $s=0$ to -4.85 kcal mol⁻¹ at $s=2$. However,
377 it significantly increases as s is growing. In particular, at $s \geq 3$ ΔG_{+A}^0 is ranging from -11.89 kcal
378 mol⁻¹ for S⁻S₃A₁ to -15.37 kcal mol⁻¹ for S⁻S₄A₁. NH₃ clearly cannot get into small negative ions.
379 However, it can easily attach to larger negative ions with $s \geq 3$ that is consistent with CLOUD



380 measurements (Schobesberger et al., 2015). Since hydration weakens NH_3 binding in $\text{S}^-\text{S}_3\text{A}_1\text{W}_w$
381 and $\text{S}^-\text{S}_4\text{A}_1\text{W}_w$ clusters, its impacts on the cluster formation and nucleation rates may potentially
382 be important.

383 In contrast to H_2O and NH_3 , binding of H_2SO_4 to small negative ions ($s < 3$) is very strong.
384 These ions are very stable even they contain no NH_3 or H_2O molecules. High electron affinity of
385 H_2SO_4 molecules results in the high stability of S^-S_s at $s=1-2$. However, the charge effect reduces
386 as s is growing. In particular, ΔG_{+S}^0 of S^-S_s drops from $-32.74 \text{ kcal mol}^{-1}$ at $s=1$ to $-10.58 \text{ kcal mol}^{-1}$
387 and $-8.28 \text{ kcal mol}^{-1}$ at $s=3$ and 4, respectively. At the same time, ΔG_{+A}^0 increases from 0.08 kcal
388 mol^{-1} ($s=1$) to $-11.89 \text{ kcal mol}^{-1}$ ($s=3$) and $-15.37 \text{ kcal mol}^{-1}$ ($s=4$). The hydration of S^-S_s at $s=3, 4$
389 enhances the strength of H_2SO_4 binding, especially at $s=4$. ΔG_{+S}^0 values for $\text{S}^-\text{S}_{3-4}\text{W}_w$ are
390 consistently $\sim 1.5 - 3 \text{ kcal mol}^{-1}$ less negative than the corresponding semi-experimental estimates
391 (Table 4). The possible reasons behind the observed systematic difference are yet to be identified
392 and include the use of low-level *ab initio* HF method to compute reaction enthalpies and
393 uncertainties in experimental enthalpies in studies by Froyd and Lovejoy (2003).

394 NH_3 binding to S^-S_3 significantly enhances the stability of H_2SO_4 in the cluster by $\sim 7 \text{ kcal mol}^{-1}$
395 compared to ΔG_{+S}^0 for the corresponding binary counterpart. The binding of the second NH_3 to
396 $\text{S}^-\text{S}_3\text{A}$ to form $\text{S}^-\text{S}_3\text{A}_2$ is much weaker ($\Delta G_{+A}^0 = -7.27 \text{ kcal mol}^{-1}$) than that of the first NH_3 molecule
397 ($\Delta G_{+A}^0 = -11.89 \text{ kcal mol}^{-1}$). This indicates that most of S^-A_a can only contain one NH_3 molecule,
398 in a perfect agreement with the laboratory study of Schobesberger et al. (2015). In the case of S^-
399 S_4 , binding of the first ($\Delta G_{+A}^0 = -15.37 \text{ kcal mol}^{-1}$) and second (and $-12.23 \text{ kcal mol}^{-1}$) NH_3
400 molecules to the cluster is quite strong, while the attachment of NH_3 leads to substantial
401 stabilization of H_2SO_4 in the cluster, as evidenced by ΔG_{+S}^0 growing from $-8.28 \text{ kcal mol}^{-1}$ at $a=0$
402 to $-11.76 \text{ kcal mol}^{-1}$ and $-16.71 \text{ kcal mol}^{-1}$ at $a=1$ and $a=2$, respectively. The NH_3 binding free
403 energy to $\text{S}^-\text{S}_4\text{A}_2$ (to form $\text{S}^-\text{S}_4\text{A}_3$) drops to $-7.59 \text{ kcal mol}^{-1}$, indicating, in agreement with the
404 CLOUD measurements (Schobesberger et al., 2015) that most of S^-S_4 clusters contain 1 or 2 NH_3
405 molecules.

406

407 2.4. Nucleation barriers for neutral/charged clusters and size-dependent evaporation rates

408 Nucleation barriers and cluster evaporation rates are critically important for calculations of
409 nucleation rates. This section describes the methods employed to calculate the evaporation rates
410 of nucleating clusters of variable sizes and compositions (i.e., γ in Eqs. 1-6) in the TIMN model.

411

412 2.4.1 Equilibrium distributions of small binary and ternary clusters

413 In the atmosphere, $[\text{H}_2\text{O}]$ is much higher than $[\text{H}_2\text{SO}_4]$ and, thus, H_2SO_4 clusters/particles are
414 always in equilibrium with water vapor (Yu, 2007). In the lower troposphere, where most of the
415 nucleation events were observed, $[\text{H}_2\text{SO}_4]$ is typically at sub-ppt to ppt level, while $[\text{NH}_3]$ is in the



416 range of sub-ppb to ppb levels (note that, in what follows, all references to vapor mixing ratios –
417 parts per billion and parts per trillion – are by volume). This means that small ternary clusters can
418 be considered to be in equilibrium with H₂O and NH₃ vapors. Like the previous BIMN model
419 derived assuming equilibrium of binary clusters with water vapor, the present TIMN model treats
420 small clusters containing a given number of H₂SO₄ molecules as being in equilibrium with both
421 H₂O and NH₃. Their relative concentrations are calculated using the thermodynamic data shown
422 in Tables 1-4.

423 Figure 3 shows the relative abundance (or molar fractions) of small positive, negative, and
424 neutral clusters ($f_{s,a,w}^{+, -, 0}$) containing a given number of H₂SO₄ molecules at the ambient temperature
425 of 292 K and three different combinations of RH and [NH₃] values. As a result of relative
426 instability of H₂SO₄ in H⁺A₁W_wS₁ compared to H⁺W_wS₁ or H⁺A₂W_wS₁ (Fig. 2c), most of positive
427 ions with one H₂SO₄ molecule exist in the form of either as H⁺W_wS₁ or H⁺A₂W_wS₁ (i.e., containing
428 either zero or two NH₃ molecules, Fig. 3a). When [NH₃]=0.3 ppb (with T=292 K), most of the
429 positive ions containing one H₂SO₄ molecule do not contain NH₃ and their composition is
430 dominated by H⁺W_wS₁ ($\bar{w} \approx 7$). At the given T and [NH₃]=0.3 ppb, around 17% of positive ions
431 with one H₂SO₄ molecule contain two NH₃ molecules at RH=38%. The fraction of positive ions
432 containing one H₂SO₄ and two NH₃ molecules decreases to 0.9%, when RH = 90%. At T=292 K
433 and RH=38%, the increase in [NH₃] by a factor of 10 to 3 ppb leads to the domination of
434 H⁺A₂W_wS₁ (~95%) in the composition of positively charged H₂SO₄ monomers. As expected, the
435 composition of positive ions and their contribution to nucleation depends on T, RH, and [NH₃].
436 The incorporation of the quantum chemical and experimental clustering thermodynamics in the
437 framework of the kinetic nucleation model enables us to study all these dependencies.

438 As a result of very weak binding of H₂O and NH₃ to small negative ions (Table 4), nearly all
439 negatively charged clusters with s=0-1 do not contain water and ammonia (not shown). In the case,
440 when s is growing to 2, all S⁻S₂A_aW_w clusters still do not contain NH₃ (i.e., a=0), while only 20-
441 40% of them contain one water molecule (w=1) (Fig. 3b). As s further increases to 3, NH₃ begins
442 to get into some of the negatively charged ions. The fraction of S⁻S₃A_aW_w clusters containing one
443 NH₃ molecule is 9% at RH=38% and [NH₃]=0.3ppb, 3% at RH=90% and [NH₃]=0.3 ppb, and
444 50% at RH=38% and [NH₃]=3 ppb. Most of S⁻S₃W_w clusters are hydrated while the fraction of S⁻
445 S₃A_aW_w clusters containing two NH₃ molecules at these ambient conditions is negligible. The
446 fraction of negative cluster ions containing two NH₃ molecules becomes significant at s=4 (Fig.
447 3b) and increases from 28% at [NH₃]=0.3 ppb to 80% at [NH₃]=3 ppb at RH=38%. At [NH₃]=0.3
448 ppb, the increase in RH from 38% to 90% reduces the fraction of NH₃ containing S⁻S₃A_aW_w
449 clusters (i.e., a>=1) from 95% to 70%, demonstrating a significant impact of RH on cluster
450 compositions and emphasizing the importance of accounting for the RH in calculations of ternary
451 nucleation rates.



452 The equilibrium distributions of neutral clusters are presented in Fig. 3c (H₂SO₄ monomers
 453 and dimers) and Fig. 3d (H₂SO₄ trimers and tetramers). Hydration is accounted for in the case of
 454 monomers and dimers and not included, due to lack of thermodynamic data, in calculations for
 455 trimers and tetramers. Based on the thermodynamic data shown in Table 3, the dominant fraction
 456 of neutral monomers is hydrated (79% at RH=38% and 94% at RH=90%) while the fraction of
 457 monomers containing NH₃ is negligible (0.02% at [NH₃]=0.3 ppb and 0.2% at [NH₃]=3 ppb,
 458 RH=38%). As a result of the growing binding strength of NH₃ with the cluster size (Table 3), the
 459 fraction of neutral sulfuric acid dimers containing one NH₃ molecule reaches 18% at [NH₃]=0.3
 460 ppb and 69% at [NH₃]=3 ppb when T=292 K and RH=38%. In the case of H₂SO₄ trimers and
 461 tetramers, data shown in Figure 3d are limited to the relative abundance of unhydrated clusters
 462 only. Under the given conditions, most of trimers contain two NH₃ molecules while most tetramers
 463 contain 3 NH₃ molecules. At [NH₃]=3 ppb, ~2% of trimers contain three NH₃ molecules (i.e.,
 464 $s=a=3$) and 55% of tetramers contain four NH₃ molecules (i.e., $s=a=4$). As a result of a significant
 465 drop of ΔG_{+A}^0 in the case, when a/s ratio exceeds one (Table 3), the fraction of neutral clusters with
 466 $a=s+1$ are negligible. The cluster distributions clearly indicate that small sulfuric acid clusters are
 467 still not fully neutralized by NH₃ even if [NH₃] is at ppb level; and that the degree of neutralization
 468 (i.e., $a:s$ ratio) increases with the cluster size.

469

470 2.4.2 Mean stepwise and accumulative Gibbs free energy change and impact of ammonia

471 In the TIMN model, the equilibrium distributions are used to calculate number concentrations
 472 weighted stepwise Gibbs free energy change for adding one H₂SO₄ molecule to form a neutral,
 473 positively charged, and negatively charged cluster containing s H₂SO₄ molecules ($\overline{\Delta G}_{s-1,s}$):

$$474 \quad \overline{\Delta G}_{s-1,s}^{+,-,0} = \sum_{a,w} f_{s,a,w}^{+,-,0} \Delta G_{s-1,s,a,w}^{+,-,0} \quad (9)$$

475 where $f_{s,a,w}^{+,-,0}$ is the equilibrium fraction of a particular cluster within a cluster type as shown in
 476 Fig. 3.

477 In the atmosphere, where substantial nucleation is observed, the sizes of critical clusters are
 478 generally small ($s < \sim 5-10$) and nucleation rates are largely controlled by the stability (or γ) of
 479 small clusters with $s < \sim 5-10$. QC calculations and experimental data on clustering
 480 thermodynamics available for clusters of small sizes (Tables 2–4), are critically important as the
 481 formation of these small clusters is generally the limiting step for nucleation. Nevertheless,
 482 thermodynamics data for larger clusters are also needed to develop a robust nucleation model that
 483 can calculate nucleation rates under various conditions. Both measurements and QC calculations
 484 (Tables 2–4) show significant effects of charge and charge signs (i.e., positive or negative) on the
 485 stability and composition of small clusters. These charge effects decrease quickly as the clusters
 486 grow, due to the short-ranged nature of dipole-charge interaction and the quick decrease of



487 electrical field strength around charged clusters as cluster sizes increase (Yu, 2005). Based on
 488 experimental data (Kearle et al., 1967; Davidson et al., 1977; Wlodek et al., 1980; Holland and
 489 Castleman, 1982; Froyd and Lovejoy, 2003), the stepwise ΔG values for clusters decreases
 490 exponentially as the cluster sizes increase and approaches to the bulk values when clusters
 491 containing more than ~ 8 -10 molecules (Yu, 2005). Cluster compositions measured with an
 492 atmospheric pressure interface time-of-flight (APi-TOF) mass spectrometer during CLOUD
 493 experiments also show that the chemical effect of charge-carrying becomes unimportant when the
 494 cluster contains more than 9 H_2SO_4 molecules (Schobesberger et al., 2015).

495 In the present TIMN model, we assume that both neutral and charged clusters have the same
 496 composition when $s \geq 10$ and the following extrapolation scheme is used to calculate $\Delta G_{s-1,s}$ for
 497 clusters up to $s=10$:

$$498 \quad \Delta G_{s-1,s} = \Delta G_{s_1-1,s_1} + \frac{\left(\Delta G_{s_2-1,s_2} - \Delta G_{s_1-1,s_1}\right)\left(e^{-s_2c} - e^{-s_1c}\right)}{\left(e^{-s_2c} - e^{-s_1c}\right)} \quad (11)$$

499 where $\Delta G_{s_1-1,s_1}$ is the stepwise mean Gibbs free energy change for H_2SO_4 addition for a specific
 500 type (neutral, positive, or negative) of clusters at $s=s_1$ that can be derived from QC calculation
 501 and/or experimental measurements, and $\Delta G_{s_2-1,s_2}$ is the corresponding value for clusters at $s=s_2$
 502 ($=10$ in the present study) that is calculated in the capillarity approximation accounting for the
 503 Kelvin effect. c in Eq. 11 is the exponential coefficient that determines how fast $\Delta G_{s-1,s}$
 504 approaches to bulk values as s increases. In the present study, c is estimated from $\Delta G_{s-1,s}$ at $s=2$
 505 and $s=3$ for neutral binary and ternary cluster for which experimental (Hanson and Lovejoy, 2006;
 506 Kazil et al., 2007) or quantum-chemical data (Table 3) are available.

507 For clusters with $s \geq s_2$, the capillarity approximation is used to calculate $\Delta G_{s-1,s}$ as

$$508 \quad \Delta G_{s-1,s} = -RT \ln(P/P_s) + \frac{2\sigma v_1 N_A}{r_s} \quad (12)$$

509 where P is the H_2SO_4 vapor pressure and P_s is the H_2SO_4 saturation vapor pressure over a flat
 510 surface with the same composition as the cluster. σ is the surface tension and v_1 is the volume of
 511 one H_2SO_4 molecule. r_s is the radius of the cluster and N_A is the Avogadro's number.



512 The scheme to calculate bulk $\Delta G_{s-1,s}$ ($s \geq 10$) for $\text{H}_2\text{SO}_4\text{-H}_2\text{O}$ binary clusters has been
513 described in Yu (2007). For ternary nucleation, both experiments (Schobesberger et al., 2015) and
514 QC calculations (Table 4) indicate that the growth of relatively large clusters follows the $s=a$ line
515 (i.e. in the composition of ammonia bisulfate). In the present TIMN model, the bulk $\Delta G_{s-1,s}$
516 values for ternary clusters are calculated based on measured H_2SO_4 saturation vapor pressure over
517 ammonia bisulfate from Martin et al. (1997) and surface tension from Hyvarinen et al. (2005).
518 Figure 4 presents stepwise ($\overline{\Delta G_{s-1,s}}$) and cumulative (total) $\overline{\Delta G_s}$ Gibbs free energy changes
519 associated with the formation of neutral, positively charged, and negatively charged binary and
520 ternary clusters containing s H_2SO_4 molecules under the conditions specified in the figure caption.
521 The clusters are assumed to be in equilibrium with water (Yu, 2007) and ammonia (Fig. 3). As
522 seen from Fig. 4, the presence of NH_3 reduces the mean $\overline{\Delta G_{s-1,s}}$ for larger clusters, which can be
523 treated as the bulk binary $\text{H}_2\text{SO}_4\text{-H}_2\text{O}$ solution (Schobesberger et al., 2015), by $\sim 3 \text{ kcal mol}^{-1}$,
524 consistent with the laboratory measurements (Marti et al., 1997) indicating a substantial reduction
525 in the H_2SO_4 vapor pressure over ternary solutions. The comparison also shows that the influence
526 of NH_3 on $\overline{\Delta G_{s-1,s}}$ of small clusters ($s \leq 4$) is much lower than that on larger ones and bulk
527 solutions. For example, at $[\text{NH}_3]=0.3 \text{ ppb}$, the differences in $\overline{\Delta G_{s-1,s}}$ between binary and ternary
528 positive ions with $s=1$ and neutral clusters with $s=2$ are only $0.45 \text{ kcal mol}^{-1}$ and $\sim 1 \text{ kcal mol}^{-1}$,
529 respectively. In the case of negative ions, zero and $0.27\text{--}0.45 \text{ kcal mol}^{-1}$ differences at $s \leq 2$ and
530 $s=3\text{--}4$, respectively, were observed. The reduced effect of ammonia on smaller clusters is explained
531 (Tables 2-S4) by ammonia's weaker bonding to smaller clusters than to larger ones, which in turn
532 yields lower average NH_3 to H_2SO_4 ratios (Fig. 3).
533 As seen from Fig. 4, bonding of H_2SO_4 to small negatively charged clusters ($s < 3$) is much
534 stronger than that to neutrals and positive ions. As a result, at $s < 3$ the formation of negatively
535 charged clusters is barrierless ($\overline{\Delta G_{s-1,s}} < 0$). $\overline{\Delta G_{s-1,s}}$ (Fig. 4a), and with growing s first increases
536 and then decreases, reaching the maximum barrier values at $s = \sim 3 - 6$. The effect of NH_3 on
537 negative ions becomes important at $s \geq 4$, when bonding between the clusters and NH_3 becomes
538 strong enough to contaminate a large fraction of binary clusters with ammonia (Fig. 3). In contrast,
539 the impact of NH_3 on neutral dimers and positively charged monomers of H_2SO_4 , as well as on



540 $\overline{\Delta G}_{s-1,s}$ for both positively charged and neutral clusters, monotonically decreases for all s ,
 541 including $s \leq 5$.

542 $\overline{\Delta G}_{s-1,s}$ for charged and neutral clusters converge into the bulk values at $s \sim 10$, when impact
 543 of the chemical identity of the core ion on the cluster composition becomes diffuse (Schobesberger
 544 et al., 2015) and when the contribution of the electrostatic effect to $\overline{\Delta G}_{s-1,s}$ becomes less than \sim
 545 $0.5 \text{ kcal mol}^{-1}$. The comparison of cumulative (total) $\overline{\Delta G}_s$ (Fig. 4b) indicates the lowest nucleation
 546 barrier for the case of negative ions, followed by positive ions and neutrals. The barrierless
 547 formation of clusters with s ranging from 1 to 3 substantially reduces the nucleation barrier for
 548 negatively charged ions and facilitates their nucleation. The presence of 0.3 ppb of NH_3 lowers the
 549 nucleation barrier for negative, positive and neutral clusters from $\sim 17, 24$ and 38 kcal mol^{-1} to 2,
 550 7 and 16 kcal mol^{-1} , respectively. A relatively low nucleation barrier for charged ternary clusters
 551 is explained by the simultaneous effect of ionization and NH_3 which also reduces the size of the
 552 critical cluster (s^*).

553 It is important to note that the size of the critical cluster, commonly used to “measure” the
 554 activity of nucleation agents in the classical nucleation theory (Coffman and Hegg, 1995;
 555 Korhonen et al., 1999; Vehkamäki et al., 2002; Napari et al., 2002; Hamill et al., 1982) is no longer
 556 a valid indicator, when charged molecular clusters and small nanoparticles are considered. As seen
 557 from Fig. 4, positively charged ternary critical clusters ($s^*=3-4$) are smaller than the corresponding
 558 negatively charged ones ($s^*=4-5$); however, the nucleation barrier for ternary positive clusters
 559 under the condition is more than three times higher than that for ternary negatives ones.

560

561 2.4.3 Size- and composition- dependent H_2SO_4 evaporation rates

562 As we mentioned earlier, H_2SO_4 is the key atmospheric nucleation precursor driving the
 563 formation and growth of clusters in the ternary $\text{H}_2\text{SO}_4\text{-H}_2\text{O-NH}_3$ system while ions, H_2O , and
 564 NH_3 act to stabilize the H_2SO_4 clusters. The clustering thermodynamic data derived from QC
 565 calculations and measurements (Section 2.3) are used to constrain size- and composition-
 566 dependent evaporation rates of H_2SO_4 which are critically important. Similar to $\overline{\Delta G}_{s-1,s}$, average
 567 or effective rates of H_2SO_4 molecule evaporation from positively charged, negatively charged, and
 568 neutral clusters containing s H_2SO_4 molecules ($\bar{\gamma}_s^{+,-,0}$) are calculated as:

$$569 \quad \bar{\gamma}_s^{+,-,0} = \sum_{a,w} f_{s,a,w}^{+,-,0} \gamma_{s,a,w}^{+,-,0} \quad (10)$$



570 where $\gamma_{s,a,w}^{+,-,0}$ is the H₂SO₄ evaporation coefficient from a particular cluster within a cluster type as
 571 shown in Fig. 3, which can be calculated based on Eq. (7) with ΔG_{+s}^0 from Tables 2-4.

572 Figure 5 gives the number concentration weighted mean evaporation rate ($\bar{\gamma}$) of an H₂SO₄
 573 molecule from these clusters under the conditions corresponding to Fig. 4. The shapes of $\bar{\gamma}$ curves
 574 are similar to those of $\overline{\Delta G}_{s-1,s}$ (Fig. 4a) as $\bar{\gamma}$ values are largely controlled by $\overline{\Delta G}_{s-1,s}$ (Eq. 7). The
 575 presence of ammonia, as expected, significantly reduces the vapor pressure of H₂SO₄ over bulk
 576 aerosol (Marti et al., 1997), and, hence, the H₂SO₄ evaporation rate. The evaporation rates of both
 577 neutral and positive clusters decrease as s increases, and the positive clusters are uniformly more
 578 stable than corresponding neutral clusters. $\bar{\gamma}$ for negative ions first increases and then decreases as
 579 s increases, peaking around $s \sim 3 - 6$. The presence of NH₃ reduces the evaporation rates of larger
 580 clusters by more than two orders of magnitude and the effect decreases for smaller clusters, as the
 581 binding of NH₃ to small neutral and charged clusters are weaker compared to that for larger clusters
 582 (Fig. 4). [NH₃] influences the average NH₃:H₂SO₄ ratio (Fig. 3) and the evaporation rates of these
 583 small clusters. The nucleation rates, limited by formation of small clusters ($s < \sim 5$), depend strongly
 584 on the stability or evaporation rate of these small clusters and, thus, on [NH₃].

585

586 3. TIMN rates and comparisons with CLOUD measurements

587 The evolution of cluster/particle size distributions can be obtained by solving the dynamic
 588 equations 1-6. Since the concentrations of clusters of all sizes are explicitly predicted, the
 589 nucleation rates in the kinetic model can be calculated for any cluster size larger than the critical
 590 size of neutral clusters ($i > i^*$) (Yu, 2006b),

$$591 \quad J_i = J_i^+ + J_i^- + J_i^0 = \beta_{i,1}^+ N_1^0 N_i^+ - \gamma_i^+ N_{i+1}^+ + \beta_{i,1}^- N_1^0 N_i^- - \gamma_i^- N_{i+1}^- + \beta_{i,1}^0 N_1^0 N_i^0 - \gamma_i^0 N_{i+1}^0 \quad (13)$$

592 where J_i^+ , J_i^- , and J_i^0 are nucleation rates associated with positive, negative, and neutral clusters
 593 containing i H₂SO₄ molecules. As a result of scavenging by pre-existing particles or wall loss, the
 594 steady state J_i decreases as i increases. To compare with CLOUD measurements, we calculate
 595 nucleation at cluster mobility diameter of 1.7 nm ($J_{1.7}$).

596 Many practical applications require information on the steady state nucleation rates. For each
 597 nucleation case presented in this paper, constant values of [H₂SO₄] (i.e., N_1^0), [NH₃], T, RH, Q,

598 and $L_i^{+,-,0}$ are assumed. The pre-existing particles with fixed surface area or wall loss serve as a
 599 sink for all clusters. Under a given condition, cluster distribution and nucleation rate reach steady
 600 state after a certain amount of time. We calculate size-dependent coefficients for a given case, and



601 then solve equations (1-6) to obtain the steady state cluster distribution and nucleation rate, with
602 the approach described in Yu (2006b).

603 Figure 6 shows a comparison of the model TIMN rates $J_{1,7}$ with CLOUD measurements, as a
604 function of $[\text{NH}_3]$ under two ionization rates. It should be noted that Dunne et al. (2016) developed
605 a simple empirical parameterization (denoted thereafter as “CLOUDpara”) of binary, ternary and
606 ion-induced nucleation rates in CLOUD measurements as a function of $[\text{NH}_3]$, $[\text{H}_2\text{SO}_4]$, T, and
607 negative ion concentration. The predictions based on CLOUDpara (Dunne et al., 2016) and ACDC
608 (McGrath et al., 2012; Kurten et al., 2016) are also presented in Fig. 6 for comparisons.

609 Like the CLOUD measurements, the TIMN predictions reveal a complex dependence of $J_{1,7}$
610 on $[\text{NH}_3]$, and an analysis of the TIMN results shows this behavior can be explained by the
611 differing responses of negative, positive and neutral clusters to the presence of ammonia (Fig. 4).
612 Under the conditions specified in Fig. 6, nucleation is dominated by negative ions for $[\text{NH}_3] < \sim 0.5$
613 ppb, by both negative and positive ions for $[\text{NH}_3]$ from ~ 0.5 ppb to ~ 10 ppb (with background
614 ionization), or ~ 20 ppb (with pion-enhanced ionization), and by neutrals at higher $[\text{NH}_3]$.
615 According to TIMN, $[\text{NH}_3]$ of at least 0.6–1 ppb are needed before positive ions contribute
616 significantly to nucleation rates – in good agreement with the threshold found in the CLOUD
617 experiments (Kirkby et al., 2011; Schobesberger et al., 2015). TIMN simulations also extend
618 CLOUD data at $[\text{NH}_3]$ of ~ 1 ppb to include a “zero-sensitivity zone” in the region of 1-10 ppb,
619 followed by a region of strong sensitivity of $J_{1,7}$ to $[\text{NH}_3]$ commencing at $[\text{NH}_3] > \sim 10$ -20 ppb. The
620 latter zone may have important implications for NPF in heavily polluted regions, including much
621 of India and China, where $[\text{NH}_3]$ may exceed 10-20 ppb (Behera and Sharma, 2010; Meng et al.,
622 2017). It is noteworthy in Fig. 6 that the dependence of $J_{1,7}$ on $[\text{NH}_3]$ and Q predicted by the ACDC
623 model (McGrath et al., 2012) and the CLOUD data parameterization (Dunne et al., 2016) deviate
624 substantially from the experimental data as well as the TIMN simulations. The CLOUDpara does
625 not consider impacts of positive ions and such key controlling parameters as RH and surface area
626 of pre-existing particles. Dunne et al. (2016) reported that CLOUDpara is also very sensitive to
627 the approach to parameterize T dependence, showing that the contribution of ternary ion-induced
628 nucleation to NPF below 15 km altitude has grown from 9.6% to 37.5%, after the initial empirical
629 temperature function was replaced with a simpler one.

630 Figure 7 presents a more detailed comparison of TIMN simulations with CLOUD
631 measurements of $J_{1,7}$ as a function of $[\text{H}_2\text{SO}_4]$, T, and RH. The TIMN model accurately reproduces
632 both the absolute values of $J_{1,7}$ and its dependencies on $[\text{H}_2\text{SO}_4]$, T, and RH, in a wide range of
633 temperatures ($T=208 - 292$ K) and $[\text{H}_2\text{SO}_4]$ ($5 \times 10^5 - 5 \times 10^8 \text{ cm}^{-3}$). As expected, nucleation rates
634 are very sensitive to $[\text{H}_2\text{SO}_4]$ and T. For example, $J_{1,7}$ increases by three to five orders of magnitude
635 with an increase in $[\text{H}_2\text{SO}_4]$ of a factor of 10, and by roughly one order of magnitude for a
636 temperature decrease of 10 degree, except in cases where the nucleation rate is limited by Q (for



637 example, $[\text{H}_2\text{SO}_4] \approx 10^8 - 10^9 \text{ cm}^{-3}$ at $T=278 \text{ K}$ and 292 K , shown in Fig. 7a). The key difference
638 between CLOUDpara and TIMN predictions is that $\text{dln}J_{1.7}/\text{dln}[\text{H}_2\text{SO}_4]$ ratio predicted by
639 CLOUDpara is nearly constant while TIMN shows that this ratio depends on both $[\text{H}_2\text{SO}_4]$ and T .
640 The CLOUD measurements taken at $T=278 \text{ K}$ clearly show (in agreement with the TIMN) that
641 $\text{dln}J_{1.7}/\text{dln}[\text{H}_2\text{SO}_4]$ is not constant. CLOUDpara overestimates $J_{1.7}$ compared to both
642 measurements and TIMN simulations, except for the case, when $T=278 \text{ K}$ and $[\text{H}_2\text{SO}_4]$ ranges
643 from $\sim 7 \times 10^6$ to $5 \times 10^7 \text{ cm}^{-3}$, with deviation of CLOUDpara from experimental data and TIMN
644 growing with the lower temperature.

645 Both CLOUD measurements and TIMN simulations (Fig. 7b) show an important influence of
646 RH on nucleation rates (which is neglected in both the CLOUDpara and ACDC models). In
647 particular, CLOUD measurements indicate 1-5 order of magnitude rise in $J_{1.7}$ after RH increases
648 from 10% to 70-80% and a stronger effect of RH on nucleation rates at higher temperatures under
649 the conditions shown in Fig. 7b. The RH dependence of $J_{1.7}$ predicted by the TIMN model is
650 consistent with measurements, being slightly weaker than the measured at high RH.

651

652 4. Summary

653 A comprehensive kinetically-based $\text{H}_2\text{SO}_4\text{-H}_2\text{O-NH}_3$ ternary ion-mediated nucleation (TIMN)
654 model, constrained with thermodynamic data from quantum-chemical calculations and laboratory
655 measurements, has been developed and used to shed a new light on physio-chemical processes
656 underlying the effect of ammonia on NPF. We show that the stabilizing effect of NH_3 grows with
657 the cluster size, and that the reduced effect of ammonia on smaller clusters is caused by weaker
658 bonding that in turn yields lower average NH_3 to H_2SO_4 ratios. NH_3 was found to impact nucleation
659 barriers for neutral, positively charged, and negatively charged clusters differently due to the large
660 difference in the binding energies of NH_3 , H_2O , and H_2SO_4 to small clusters of different charging
661 states. The lowest and highest nucleation barriers are observed in the case of negative ions and
662 neutrals, respectively. Therefore, nucleation of negative ions is favorable, followed by nucleation
663 of positive ions and neutrals. Different responses of negative, positive and neutral clusters to
664 ammonia result in a complex dependence of ternary nucleation rates on $[\text{NH}_3]$. The TIMN model
665 reproduces both the absolute values of nucleation rates and their dependencies on the key
666 controlling parameters and agrees with the CLOUD measurements much better than other models
667 being tested here over a wide range of ambient conditions encompassing those encountered in the
668 global atmosphere.

669 The TIMN model developed in the present study may be subject to uncertainties associated with
670 the use of experimental and thermodynamic data for pre-nucleation clusters. Further measurements
671 and quantum calculations are needed to reduce the uncertainties. While the TIMN model predicts
672 nucleation rates in a good agreement with the CLOUD measurements, its ability to explain the



673 NPF events observed in the real atmosphere is yet to be quantified and will be investigated in
674 further studies.

675

676 **Acknowledgments.** The authors thank Richard Turco (Distinguished Professor Emeritus, UCLA)
677 for comments that helped to improve the manuscript. This study was supported by NSF under
678 grant 1550816, NASA under grant NNX13AK20G, and NYSERDA under contract 100416. ABN
679 would like to thank the Russian Ministry of Education and Science for its support.

680

681 **Data availability.** All relevant data are available in the article, or from the corresponding authors
682 upon request.

683

684 **References**

685 Almeida, J., et al., Molecular understanding of sulphuric acid–amine particle nucleation in the
686 atmosphere, *Nature*, 502, 359-363, 2013.

687 Ball, S. M., Hanson, D. R., Eisele, F. L., and McMurry, P. H., Laboratory studies of particle
688 nucleation: Initial results for H₂SO₄, H₂O, and NH₃ vapors, *J. Geophys. Res.*, 104, 23709-23718,
689 10.1029/1999JD900411, 1999.

690 Bandy, A.R. and Ianni, J.C., Study of the hydrates of H₂SO₄ using density functional theory. The
691 *Journal of Physical Chemistry A*, 102(32), pp.6533-6539, 1998.

692 Behera, S. N., and M. Sharma, Investigating the potential role of ammonia in ion chemistry of fine
693 particulate matter formation for an urban environment, *The Science of the Total Environment*,
694 408(17), 3569-3575, 2010.

695 Benson, D. R., M. E. Erupe, and S.-H. Lee, Laboratory-measured H₂SO₄-H₂O-NH₃ ternary
696 homogeneous nucleation rates: Initial observations, *Geophys. Res. Lett.*, 36, L15818,
697 doi:10.1029/2009GL038728, 2009.

698 Bork, N., Du, L., Reiman, H., Kurtén, T. and Kjaergaard, H.G., Benchmarking ab initio binding
699 energies of hydrogen-bonded molecular clusters based on FTIR spectroscopy, *Journal of*
700 *Physical Chemistry A*, 118(28), 5316-5322, 2014.

701 Bustos, D.J., Temelso, B. and Shields, G.C., Hydration of the Sulfuric Acid–Methylamine
702 Complex and Implications for Aerosol Formation. *The Journal of Physical Chemistry A*,
703 118(35), pp.7430-7441, 2014.

704 Chen, M., M. Titcombe, J. Jiang, C. Kuang, M. L. Fischer, E. Edgerton, F. L. Eisele, J. I. Siepmann,
705 D. H. Hanson, J. Zhao, and P. H. McMurry, Acid-base chemical reaction model for nucleation
706 rates in the polluted boundary layer. *Proc. Nat. Acad. Sci.*, 109, 18713–18718, 2012.



- 707 Chon, N.L., Lee, S.H. and Lin, H., A theoretical study of temperature dependence of cluster
708 formation from sulfuric acid and ammonia. *Chemical Physics*, 433, pp.60-66, 2014.
- 709 Coffman, D. J., and Hegg, D. A., A preliminary study of the effect of ammonia on particle
710 nucleation in the marine boundary layer, *J. Geophys. Res.*, 100, 7147-7160, 1995.
- 711 Davidson, J. A., Fehsenfeld, F.C., Howard, C.J.: The heats of formation of NO_3^- and NO_3^-
712 association complexes with HNO_3 and HBr , *Int. J. Chem. Kinet.*, 9, 17, 1977.
- 713 Dawson M.L., et al., Simplified mechanism for new particle formation from methanesulfonic acid,
714 amines and water via experiments and ab initio calculations, *Proc Natl Acad Sci USA*
715 109:18719–18724, 2012.
- 716 DePalma, J.W., Bzdek, B.R., Doren, D.J. and Johnston, M.V., Structure and energetics of
717 nanometer size clusters of sulfuric acid with ammonia and dimethylamine, *Journal of Physical*
718 *Chemistry A*, 116(3), pp.1030-1040, 2012.
- 719 Doyle, G. J., Self-nucleation in the sulfuric acid-water system, *J. Chem. Phys.*, 35, 795–799, 1961.
- 720 Dunne, E. M., et al., Global particle formation from CERN CLOUD measurements, *Science*,
721 doi:10.1126/science.aaf2649, 2016.
- 722 Duplissy J., et al., Effect of ions on sulfuric acid-water binary particle formation: 2. Experimental
723 data and comparison with QC-normalized classical nucleation theory, *J. Geophys. Res. Atmos.*,
724 121, 1752–1775, doi:10.1002/2015JD023539, 2016.
- 725 Elm, J. and Mikkelsen, K.V., Computational approaches for efficiently modelling of small
726 atmospheric clusters, *Chemical Physics Letters*, 615, 26-29, 2014.
- 727 Elm, J., Bilde, M. and Mikkelsen, K.V., Assessment of binding energies of atmospherically
728 relevant clusters, *Physical Chemistry Chemical Physics*, 15(39), 16442-16445, 2013.
- 729 Elm, J., Bilde, M. and Mikkelsen, K.V., Assessment of density functional theory in predicting
730 structures and free energies of reaction of atmospheric prenucleation clusters, *Journal of*
731 *chemical theory and computation*, 8(6), 2071-2077, 2012.
- 732 Frisch, M. J., Trucks, G. W., Schlegel, H. B., Scuseria, G. E., Robb, M. A., Cheeseman, J. R.,
733 Scalmani, G., Barone, V., Mennucci, B., et al., *Gaussian 09*, Gaussian, Inc., Wallingford CT,
734 2009.
- 735 Froyd K. D., and Lovejoy E. R., Bond energies and structures of ammonia-sulfuric acid positive
736 cluster ions, *J. Phys. Chem. A*, 116(24), 5886–5899, doi:10.1021/jp209908f, 2012.
- 737 Froyd, K. D., and Lovejoy, E. R., Experimental thermodynamics of cluster ions composed of
738 H_2SO_4 and H_2O . 1. Positive ions, *J. Phys. Chem. A*, 107, 9800–9811, 2003.
- 739 Froyd, K. D., and Lovejoy, E. R., Experimental thermodynamics of cluster ions composed of
740 H_2SO_4 and H_2O . 2. Measurements and ab initio structures of negative ions, *J. Phys. Chem. A*,
741 107, 9812–9824, 2003.



- 742 Froyd, K. D., and Lovejoy, E. R., Experimental thermodynamics of cluster ions composed of
743 H₂SO₄ and H₂O. 1. Positive ions, *J. Phys. Chem. A*, 107, 9800–9811, 2003.
- 744 Froyd, K. D., Ion induced nucleation in the atmosphere: Studies of NH₃, H₂SO₄, and H₂O cluster
745 ions, Ph.D. thesis, Univ. of Colo., Boulder, 2002.
- 746 Glasoe, W. A., Volz, K., Panta, B., Freshour, N., Bachman, R., Hanson, D. R., McMurry, P. H.,
747 and Jen, C.. Sulfuric acid nucleation: An experimental study of the effect of seven bases. *Journal*
748 *of Geophysical Research: Atmospheres*, 120(5), 1933-1950, 2015.
- 749 Hamill, P., Turco, R. P., Kiang, C. S., Toon, O. B., & Whitten, R. C., An analysis of various
750 nucleation mechanisms for sulfate particles in the stratosphere. *Journal of Aerosol Science*, 13,
751 561–585, 1982.
- 752 Hanson, D. R., and F. Eisele, Diffusion of H₂SO₄ in humidified nitrogen: Hydrated H₂SO₄, *J. Phys.*
753 *Chem. A*, 104, 1715 – 1719, 2000.
- 754 Hanson, D. R., and F. L. Eisele, Measurement of prenucleation molecular clusters in the NH₃,
755 H₂SO₄, H₂O system, *J. Geophys. Res.*, 107(D12), 4158, doi:10.1029/2001JD001100, 2002.
- 756 Hanson, DR., Lovejoy, ER, Measurement of the thermodynamics of the hydrated dimer and
757 trimers, *J. Phys. Chem. A* 110: 9525-9538 DOI: 10.1021/jp062844w, 2006.
- 758 Henschel, H., J. C. A. Navarro, T. Yli-Juuti, O. Kupiainen-Määttä, T. Olenius, I. K. Ortega, S. L.
759 Clegg, T. Kurtén, I. Riipinen, and H. Vehkamäki, Hydration of atmospherically relevant
760 molecular clusters: Computational chemistry and classical thermodynamics, *J. Phys. Chem. A*,
761 118, 2599–2611, 2014.
- 762 Henschel, H., T. Kurtén, and H. Vehkamäki, Computational study on the effect of hydration on
763 new particle formation in the sulfuric acid/ammonia and sulfuric acid/dimethylamine systems,
764 *J. Phys. Chem. A*, 120, 1886–1896, doi:10.1021/acs.jpca.5b11366, 2016.
- 765 Herb, J., Y. Xu, F. Yu, and A. B. Nadykto, Large Hydrogen-Bonded Pre-Nucleation (HSO₄⁻
766)(H₂SO₄)_m(H₂O)_k and (HSO₄⁻)(NH₃)(H₂SO₄)_m(H₂O)_k Clusters in the Earth's Atmosphere, *J.*
767 *Phys. Chem., A*, 117, 133-152, DOI: 10.1021/jp3088435, 2013.
- 768 Herb, J., A. Nadykto, and F. Yu, Large Ternary Hydrogen-Bonded Pre-Nucleation Clusters in the
769 Earth's Atmosphere, *Chemical Physics Letters*, 518, 7-14, 10.1016/j.cplett.2011.10.035, 2011.
- 770 Holland, P. M., and Castleman, A. W., Jr.: Thomson equation revisited in light of ion-clustering
771 experiments, *J. Phys. Chem.*; 86, 4181-4188, 1982.
- 772 Husar, D.E., Temelso, B., Ashworth, A.L. and Shields, G.C., Hydration of the bisulfate ion:
773 atmospheric implications. *The Journal of Physical Chemistry A*, 116(21), pp.5151-5163, 2012.
- 774 Hyvärinen A., Heikki Lihavainen, Yrjö Viisanen, and Markku Kulmala, Homogeneous nucleation
775 rates of higher n-alcohols measured in a laminar flow diffusion chamber, *The Journal of*
776 *Chemical Physics* 2004 120:24, 11621-11633, 2005.



- 777 Ianni, J.C. and Bandy, A.R., A Density Functional Theory Study of the Hydrates of $\text{NH}_3\text{-H}_2\text{SO}_4$
778 and Its Implications for the Formation of New Atmospheric Particles. *The Journal of Physical*
779 *Chemistry A*, 103(15), pp.2801-2811, 1999.
- 780 Jacobson, M., Turco, R., Jensen, E. and Toon O.: Modeling coagulation among particles of
781 different composition and size, *Atmos. Environ.*, 28, 1327-1338, 1994.
- 782 Jolly, William L., *Modern Inorganic Chemistry (2nd Edn.)*. New York: McGraw-Hill. ISBN 0-07-
783 112651-1, 1991.
- 784 Kazil, J., Lovejoy, E. R., Jensen, E. J., and Hanson, D. R.: Is aerosol formation in cirrus clouds
785 possible?, *Atmos. Chem. Phys.*, 7, 1407-1413, <https://doi.org/10.5194/acp-7-1407-2007>, 2007.
- 786 Kebarle, P., S. K. Searles, A. Zolla, J. Scarborough, and M. Arshadi, *J. Am. Chem. Soc.*, 89, 6393,
787 1967.
- 788 Kim, T. O., T. Ishida, M. Adachi, K. Okuyama, and J. H. Seinfeld, *Nanometer-Sized Particle*
789 *Formation from $\text{NH}_3/\text{SO}_2/\text{H}_2\text{O}/\text{Air}$ Mixtures by Ionizing Irradiation*, *Aerosol Science and*
790 *Technology*, 29, 112-125, 1998.
- 791 Kirkby, J., Curtius, J., Almeida, J., Dunne, E., Duplissy, J., et al., The role of sulfuric acid,
792 ammonia and galactic cosmic rays in atmospheric aerosol nucleation, *Nature*, 476, 429-433,
793 2011.
- 794 Korhonen, P., Kulmala, M., Laaksonen, A., Viisanen, Y., McGraw, R., and Seinfeld, J. H., Ternary
795 nucleation of H_2SO_4 , NH_3 , and H_2O in the atmosphere, *J. Geophys. Res.*, 104, 26,349-26,353,
796 1999.
- 797 Kürten, A., et al., Experimental particle formation rates spanning tropospheric sulfuric acid and
798 ammonia abundances, ion production rates, and temperatures, *J. Geophys. Res. Atmos.*, 121,
799 12,377-12,400, doi:10.1002/2015JD023908, 2016.
- 800 Kürten, A., Münch, S., Rondo, L., Bianchi, F., Duplissy, J., Jokinen, T., Junninen, H., Sarnela, N.,
801 Schobesberger, S., Simon, M. and Sipilä, M., Thermodynamics of the formation of sulfuric acid
802 dimers in the binary ($\text{H}_2\text{SO}_4\text{-H}_2\text{O}$) and ternary ($\text{H}_2\text{SO}_4\text{-H}_2\text{O-NH}_3$) system. *Atmospheric*
803 *Chemistry and Physics*, 15(18), pp.10701-10721, 2015.
- 804 Laakso, L., Mäkelä, J. M., Pirjola, L., and Kulmala, M., Model studies of ion-induced nucleation
805 in the atmosphere, *J. Geophys. Res.*, 107, 4427, doi:10.1029/2002JD002140, 2003.
- 806 Leverentz, H.R., Siepmann, J.I., Truhlar, D.G., Loukonen, V. and Vehkamäki, H., Energetics of
807 atmospherically implicated clusters made of sulfuric acid, ammonia, and dimethyl amine,
808 *Journal of Physical Chemistry A*, 117(18), 3819-3825, 2013.
- 809 Lovejoy, E. R., Curtius, J., and Froyd, K. D., Atmospheric ion-induced nucleation of sulfuric acid
810 and water, *J. Geophys. Res.*, 109, D08204, doi:10.1029/2003JD004460, 2004.



- 811 Ma, Y., Chen, J., Jiang, S., Liu, Y.R., Huang, T., Miao, S.K., Wang, C.Y. and Huang, W.,
812 Characterization of the nucleation precursor (H₂SO₄-(CH₃)₂NH) complex: intra-cluster
813 interactions and atmospheric relevance. RSC Advances, 6(7), pp.5824-5836, 2016.
- 814 Marti, J. J., A. Jefferson, X. Ping Cai, C. Richert, P. H. McMurry, and F. Eisele, H₂SO₄ vapor
815 pressure of sulfuric acid and ammonium sulfate solutions, J. Geophys. Res., 102(D3), 3725–3736,
816 1997.
- 817 McGrath, M. J., Olenius, T., Ortega, I. K., Loukonen, V., Paasonen, P., Kurtén, T., Kulmala, M.,
818 and Vehkamäki, H.: Atmospheric Cluster Dynamics Code: a flexible method for solution of the
819 birth-death equations, Atmos. Chem. Phys., 12, 2345-2355, doi:10.5194/acp-12-2345-2012,
820 2012.
- 821 Meng, Z., Xu, X., Lin, W., Xie, Y., Song, B., Jia, S., Zhang, R., Peng, W., Wang, Y., Cheng, H.,
822 Yang, W., and Zhao, H., Role of ambient ammonia in particulate ammonium formation at a rural
823 site in the North China Plain, Atmos. Chem. Phys. Discuss., [https://doi.org/10.5194/acp-2017-](https://doi.org/10.5194/acp-2017-174)
824 174, in review, 2017.
- 825 Meot-Ner (Mautner), M., The Ionic Hydrogen Bond and Ion Solvation. 2. Hydration of Onium
826 Ions by 1 - 7 H₂O Molecules. Relations Between Monomolecular, Specific and Bulk Hydration,
827 J. Am. Chem. Soc., 106, 5, 1265, 1984.
- 828 Merikanto J., I. Napari, H. Vehkamäki, T. Anttila, M. Kulmala, New parameterization of sulfuric
829 acid-ammonia-water ternary nucleation rates at tropospheric conditions, J. Geophys. Res., 112,
830 D15207, doi:10.1029/2006JD007977, 2007.
- 831 Miao, S.K., Jiang, S., Chen, J., Ma, Y., Zhu, Y.P., Wen, Y., Zhang, M.M. and Huang, W.,
832 Hydration of a sulfuric acid–oxalic acid complex: acid dissociation and its atmospheric
833 implication, RSC Advances, 5(60), 48638-48646, 2015.
- 834 Nadykto, A. B., A. Al Natsheh, F. Yu, K.V. Mikkelsen, and J. Herb, Computational Quantum
835 Chemistry: A New Approach to Atmospheric Nucleation, Advances in Quantum Chemistry, 55,
836 449-478, 2008.
- 837 Nadykto, A. B., Al Natsheh, A., Yu, F., Mikkelsen, K. V., and Ruuskanen, J., Quantum nature of
838 the sign preference in the ion-induced nucleation, Physical Review Letters, 96, 125701, 2006.
- 839 Nadykto, A., and Yu, F., Uptake of neutral polar vapour molecules by charged particles:
840 Enhancement due to dipole-charge interaction, J. Geophys. Res., 108(D23), 4717,
841 doi:10.1029/2003JD003664, 2003.
- 842 Nadykto, A.B. and Yu, F., Strong hydrogen bonding between atmospheric nucleation precursors
843 and common organics. Chemical physics letters, 435(1), pp.14-18, 2007a.



- 844 Nadykto, A.B., Du, H. and Yu, F., Quantum DFT and DF–DFT study of vibrational spectra of
845 sulfuric acid, sulfuric acid monohydrate, formic acid and its cyclic dimer. *Vibrational*
846 *spectroscopy*, 44(2), pp.286-296, 2007b.
- 847 Nadykto, A.B., Herb, J., Yu, F. and Xu, Y., Enhancement in the production of nucleating clusters
848 due to dimethylamine and large uncertainties in the thermochemistry of amine-enhanced
849 nucleation. *Chemical Physics Letters*, 609, 42-49, 2014.
- 850 Nadykto, A.B., Herb, J., Yu, F., Nazarenko, E.S. and Xu, Y., Reply to the ‘Comment on
851 “Enhancement in the production of nucleating clusters due to dimethylamine and large
852 uncertainties in the thermochemistry of amine-enhanced nucleation”’ by Kupiainen-Maatta et al.
853 *Chemical Physics Letters*, 624, 111-118, 2015.
- 854 Napari, I, Noppel, M, Vehkamäki, H., Kulmala, M., An improved model for ternary nucleation of
855 sulfuric acid–ammonia–water. *J. Chem. Phys.*, 116: 4221-4227, DOI: 10.1063/1.1450557, 2002.
- 856 Olenius T., O. Kupiainen-Määttä, I. K. Ortega, T. Kurtén, and H. Vehkamäki, Free energy barrier
857 in the growth of sulfuric acid–ammonia and sulfuric acid–dimethylamine clusters, *The Journal*
858 *of Chemical Physics* 2013 139:8, 2013.
- 859 Ortega, I. K., Kupiainen, O., Kurtén, T., Olenius, T., Wilkman, O., McGrath, M. J., Loukonen, V.,
860 and Vehkamäki, H., From quantum chemical formation free energies to evaporation rates,
861 *Atmos. Chem. Phys.*, 12, 225-235, 2012.
- 862 Payzant, J.D.; Cunningham, A.J.; Kebarle, P., Gas - Phase Solvation of Ammonium Ion by NH₃
863 and H₂O and Stabilities of Mixed Clusters NH₄⁺(NH₃)_n(H₂O)_w, *Can. J. Chem.*, 51, 19, 3242,
864 1973.
- 865 Peng, X.Q., Liu, Y.R., Huang, T., Jiang, S. and Huang, W., Interaction of gas phase oxalic acid
866 with ammonia and its atmospheric implications, *Physical Chemistry Chemical Physics*, 17(14),
867 9552-9563, 2015.
- 868 Raes, F., A. Janssens, and R. V. Dingenen, The role of ion-induced aerosol formation in the lower
869 atmosphere, *J. Aerosol Sci.*, 17, 466–470, 1986.
- 870 Schnitzhofer, R., et al., Characterisation of organic contaminants in the CLOUD chamber at
871 CERN, *Atmos. Meas. Tech.*, 7, 2159–2168, doi:10.5194/amt-7-2159-2014, 2014.
- 872 Schobesberger, S., et al., On the composition of ammonia–sulfuric-acid ion clusters during aerosol
873 particle formation, *Atmos. Chem. Phys.*, 15, 55-78, <https://doi.org/10.5194/acp-15-55-2015>,
874 2015.
- 875 Sorokin, A., Arnold, F. and Wiedner, D., Formation and growth of sulfuric acid–water cluster ions:
876 Experiments, modelling, and implications for ion-induced aerosol formation, *Atmospheric*
877 *Environment*, 40, 2030-2045, 2006.



- 878 Temelso, B., Morrell, T.E., Shields, R.M., Allodi, M.A., Wood, E.K., Kirschner, K.N.,
879 Castonguay, T.C., Archer, K.A. and Shields, G.C., Quantum mechanical study of sulfuric acid
880 hydration: Atmospheric implications. *The Journal of Physical Chemistry A*, 116(9), 2209-2224,
881 2012a.
- 882 Temelso, B., Phan, T.N. and Shields, G.C., Computational study of the hydration of sulfuric acid
883 dimers: Implications for acid dissociation and aerosol formation, *Journal of Physical Chemistry*
884 *A*, 116(39), pp.9745-9758, 2012b.
- 885 Thomson, J. J., *Applications of Dynamics to Physics and Chemistry*, 1st ed., Cambridge University
886 Press, London, 1888.
- 887 Torpo, L., Kurtén, T., Vehkamäki, H., Laasonen, K., Sundberg, M.R. and Kulmala, M.,
888 Significance of ammonia in growth of atmospheric nanoclusters. *The Journal of Physical*
889 *Chemistry A*, 111(42), pp.10671-10674, 2007.
- 890 Vehkamäki H., Kulmala, M., Napari, I., Lehtinen, K. E. J., Timmreck, C., Noppel, M., and
891 Laaksonen, A., An improved parameterization for sulfuric acid–water nucleation rates for
892 tropospheric and stratospheric conditions, *J. Geophys. Res.*, 107 (D22), 4622,
893 doi:10.1029/2002JD002184, 2002.
- 894 Wilhelm, S., Eichkorn, S., Wiedner, D., Pirjola, L. and Arnold, F.: Ion-induced aerosol formation:
895 new insights from laboratory measurements of mixed cluster ions, $\text{HSO}_4^-(\text{H}_2\text{SO}_4)_a(\text{H}_2\text{O})_w$ and
896 $\text{H}^+(\text{H}_2\text{SO}_4)_a(\text{H}_2\text{O})_w$, *Atmos. Environ.*, 38, 1735-1744, 2004.
- 897 Włodek, S., Z. Łuczyński, H. Wincel, Stabilities of gas-phase $\text{NO}_3^- (\text{HNO}_3)_n$, $n \leq 6$, clusters, In
898 *International Journal of Mass Spectrometry and Ion Physics*, 35, 1–2, 1980, 39-46, 1980.
- 899 Xu, W. and Zhang, R., A theoretical study of hydrated molecular clusters of amines and
900 dicarboxylic acids, *Journal of chemical physics*, 139(6), p.064312, 2013.
- 901 Xu, W. and Zhang, R., Theoretical investigation of interaction of dicarboxylic acids with common
902 aerosol nucleation precursors, *Journal of Physical Chemistry A*, 116(18), 4539-4550, 2012.
- 903 Yu, F., and Turco, R. P., The role of ions in the formation and evolution of particles in aircraft
904 plumes, *Geophys. Res. Lett.*, 24, 1927-1930, 1997.
- 905 Yu, F., and Turco, R. P., Ultrafine aerosol formation via ion-mediated nucleation, *Geophys. Res.*
906 *Lett.*, 27, 883-886, 2000.
- 907 Yu, F., and R. P. Turco: From molecular clusters to nanoparticles: The role of ambient ionization
908 in tropospheric aerosol formation, *J. Geophys. Res.*, 106, 4797-4814, 2001.
- 909 Yu, F. and Turco, R. P., The size-dependent charge fraction of sub-3-nm particles as a key
910 diagnostic of competitive nucleation mechanisms under atmospheric conditions, *Atmos. Chem.*
911 *Phys.*, 11, 9451–9463, doi:10.5194/acp-11-9451-2011, 2011.



- 912 Yu, F., Modified Kelvin-Thomson equation considering ion-dipole interaction: Comparison with
913 observed ion-clustering enthalpies and entropies, *J. Chem. Phys.*, 122, 084503, 2005.
- 914 Yu, F., Effect of ammonia on new particle formation: A kinetic H₂SO₄-H₂O-NH₃ nucleation model
915 constrained by laboratory measurements, *J. Geophys. Res.*, 111, D01204,
916 doi:10.1029/2005JD005968, 2006a.
- 917 Yu, F., From molecular clusters to nanoparticles: Second-generation ion-mediated nucleation
918 model, *Atmos. Chem. Phys.*, 6, 5193-5211, 2006b.
- 919 Yu, F., Improved quasi-unary nucleation model for binary H₂SO₄-H₂O homogeneous nucleation,
920 *J. Chem. Phys.*, 127, 054301, 2007.
- 921 Zhang, R., Khalizov, A.F., Wang, L., Hu, M., Wen, X., Nucleation and growth of nanoparticles in the
922 atmosphere, *Chem. Rev.* 112: 1957-2011, DOI: 10.1021/cr2001756, 2012.
- 923 Zhang, R., Wang, L., Khalizov, A.F., Zhao, J., Zheng, J., McGraw, R.L. and Molina, L.T.,
924 Formation of nanoparticles of blue haze enhanced by anthropogenic pollution, *Proceedings of*
925 *the National Academy of Sciences*, 106(42), 17650-17654, 2009.
- 926 Zhang, Y., P. H. McMurry, F. Yu, and M. Z. Jacobson, A Comparative Study of Homogeneous
927 Nucleation Parameterizations, Part I. Examination and Evaluation of the Formulations, *J.*
928 *Geophys. Res.*, 115, D20212, doi:10.1029/2010JD014150, 2010.
- 929 Zhu, Y.P., Liu, Y.R., Huang, T., Jiang, S., Xu, K.M., Wen, H., Zhang, W.J. and Huang, W.,
930 Theoretical study of the hydration of atmospheric nucleation precursors with acetic acid, *Journal*
931 *of Physical Chemistry A*, 118(36), 7959-7974, 2014.
- 932 Zollner, J. H., W. A. Glasoe, B. Panta, K. K. Carlson, P. H. McMurry, and D. R. Hanson, Sulfuric
933 acid nucleation: Power dependencies, variation with relative humidity, and effect of bases,
934 *Atmos. Chem. Phys.*, 12(10), 4399-4411, doi:10.5194/acp-12-4399-2012, 2012.
- 935



936 **Table 1.** Number of isomers successfully converged at 6-311 level for selected clusters, along
 937 with the enthalpy (H), entropy (S), and Gibbs free energy (G) of the most stable isomers.
 938

Cluster Formula	6-311++ conv.	H	S	G
S ₄	56	-2801.256008	179.461	-2801.341276
S ₄ A ₁	169	-2857.820795	187.395	-2857.909833
S ₄ A ₂	84	-2914.388489	193.997	-2914.480663
S ₄ A ₃	68	-2970.94645	209.77	-2971.046119
S ₄ A ₄	38	-3027.500303	225.959	-3027.607663
S ₄ A ₅	34	-3084.050337	237.758	-3084.163303
S ⁻ S ₃	97	-2800.835072	168.993	-2800.915366
S ⁻ S ₃ A ₁	122	-2857.389946	184.899	-2857.477797
S ⁻ S ₃ A ₂	21	-2913.941409	192.489	-2914.032867
S ⁻ S ₃ A ₃	13	-2970.490814	195.627	-2970.583762
S ⁻ S ₄	138	-3501.162655	200.525	-3501.257931
S ⁻ S ₄ A ₁	71	-3557.727072	208.015	-3557.825907
S ⁻ S ₄ A ₂	22	-3614.287482	213.397	-3614.388874
S ⁻ S ₄ A ₃	23	-3670.836831	226.504	-3670.94445
S ⁻ S ₄ A ₄	18	-3727.385956	237.152	-3727.498634
H ⁺ A ₂	16	-113.413269	68.478	-113.445805
H ⁺ A ₂ W ₁	42	-189.845603	94.248	-189.890384
H ⁺ A ₂ W ₂	56	-266.276653	113.49	-266.330576
H ⁺ A ₂ W ₃	63	-342.706301	132.722	-342.769362
H ⁺ A ₂ W ₄	114	-419.133157	160.449	-419.209391
H ⁺ A ₂ W ₅	116	-495.567408	161.447	-495.644117
H ⁺ A ₂ W ₆	70	-571.994961	175.085	-572.078149
H ⁺ A ₂ W ₀ S ₁	40	-813.745253	107.764	-813.796455
H ⁺ A ₂ W ₁ S ₁	173	-890.181285	121.33	-890.238933
H ⁺ A ₂ W ₂ S ₁	103	-966.618165	130.584	-966.680209
H ⁺ A ₂ W ₃ S ₁	169	-1043.047622	154.145	-1043.120861
H ⁺ A ₂ W ₄ S ₁	188	-1119.476882	177.051	-1119.561004
H ⁺ A ₂ W ₅ S ₁	178	-1195.90253	200.029	-1195.99757
H ⁺ A ₂ W ₆ S ₁	85	-1272.330781	215.117	-1272.43299

939



940 **Table 2.** QC-based stepwise Gibbs free energy change for the addition of one water (ΔG_{+W}°),
 941 ammonia (ΔG_{+A}°), or sulfuric acid (ΔG_{+S}°) molecule to form the given positively charged clusters
 942 under standard conditions, and the corresponding experimental data or semi-experimental
 943 estimates.
 944

	ΔG_{+W}°		ΔG_{+A}°		ΔG_{+S}°	
	QC	experimental	QC	experimental	QC	experimental
$H^+W_1S_1$					-28.59	-24.65 ^f
$H^+W_2S_1$	-15.66				-15.33	-13.76 ^f
$H^+W_3S_1$	-9.40				-10.12	-11.93 ^f
$H^+W_4S_1$	-7.83				-9.18	-9.71 ^f
$H^+W_5S_1$	-6.77	-5.79 ^a			-9.52	-9.82 ^f
$H^+W_6S_1$	-5.32	-4.24 ^a			-9.70	-9.94 ^f
$H^+W_7S_1$	-3.18	-3.28 ^a			-9.64	-9.96 ^f
$H^+W_8S_1$	-2.80	-2.67 ^a			-9.84	-10.10 ^f
$H^+W_9S_1$	-2.30	-2.12 ^a			-10.24	-10.86 ^f
$H^+A_1W_1$	-13.47	-13.01 ^b , -11.43 ^c	-52.08			
$H^+A_1W_2$	-9.85	-7.14 ^b , -8.17 ^c	-33.02			
$H^+A_1W_3$	-6.60	-5.92 ^b , -5.88 ^c	-25.01			
$H^+A_1W_4$	-3.50	-3.94 ^b , -4.06 ^c	-19.73			
$H^+A_1W_5$	-2.50	-2.55 ^b , -3.02 ^c	-15.80			
$H^+A_1W_6$	-2.26	-2.54 ^b	-12.93			
$H^+A_1W_7$	-1.15	-1.84 ^b	-10.84			
$H^+A_1W_8$	-1.02		-9.26			
$H^+A_1W_9$	0.25		-8.32			
H^+A_2			-22.97	-18.25 ^c		
$H^+A_2W_1$	-7.04	-6.85 ^c	-16.53	-11.54 ^c , -12.75 ^d		
$H^+A_2W_2$	-4.29	-5.25 ^c	-10.97	-9.13 ^c , -9.50 ^d		
$H^+A_2W_3$	-3.41	-3.70 ^c	-7.78	-6.83 ^c , -7.02 ^d		
$H^+A_2W_4$	-3.08		-7.36			
$H^+A_2W_5$	-1.97		-6.82			
$H^+A_2W_6$	-0.42		-4.99			
$H^+A_1W_1S_1$	-8.99		-33.14		-9.65	-8.3 ^d
$H^+A_1W_2S_1$	-8.11		-25.59		-7.90	-7.1 ^d
$H^+A_1W_3S_1$	-6.09		-22.28		-7.40	-6.7 ^d
$H^+A_1W_4S_1$	-4.25		-18.71		-8.15	-6.9 ^d
$H^+A_1W_5S_1$	-1.92		-13.85		-7.56	-7.5 ^d
$H^+A_1W_6S_1$	-2.04		-10.57		-7.34	-8.0 ^d
$H^+A_2W_0S_1$			-22.09	-22.14 ^e	-13.35	-16.8 ^d



$\text{H}^+\text{A}_2\text{W}_1\text{S}_1$	-5.72	-18.92	-12.03	-15.8 ^d
$\text{H}^+\text{A}_2\text{W}_2\text{S}_1$	-4.97	-15.78	-12.71	-15.9 ^d
$\text{H}^+\text{A}_2\text{W}_3\text{S}_1$	-4.58	-14.27	-13.89	-16.3 ^d
$\text{H}^+\text{A}_2\text{W}_4\text{S}_1$	-4.26	-14.27	-15.06	-17.3 ^d
$\text{H}^+\text{A}_2\text{W}_5\text{S}_1$	-2.01	-14.37	-15.11	-18.8 ^d
$\text{H}^+\text{A}_2\text{W}_6\text{S}_1$	-1.29	-13.63	-15.98	-19.9 ^d

945 ^a Froyd and Lovejoy, 2003; ^b Meot-Ner (Mautner) et al., 1984; ^c Payzant et al., 1973; ^d Froyd, 2002; ^e

946 Froyd and Lovejoy, 2012. ^f The ΔG_{+S}^0 values given here were calculated based experimental ΔG_{+S}^0 values

947 at T=270 K from Froyd and Lovejoy (2003) and ΔS values from quantum calculation.

948

949 **Table 3.** Same as Table 2 except for neutral clusters.

950

	ΔG_{+W}°		ΔG_{+A}°		ΔG_{+S}°	
	QC	experimental	QC	experimental	QC	experimental
S_1A_1			-7.77 ^a (-7.29 ^b , -7.61 ^c , -6.60 ^d)	-8.2 ^e	-7.77 ^a (-7.29 ^b , -7.61 ^c , -6.60 ^d)	-8.2 ^e
$S_1A_1W_1$	-1.39 ^a		-6.88 ^a			
$S_1A_1W_2$	-2.30 ^a		-6.18 ^a			
$S_1A_1W_3$	-1.52 ^a		-5.81 ^a			
S_1A_2			-4.75			
$S_1A_2W_1$	-0.78		-4.15			
S_2A_1			-13.84 ^a		-11.65 ^a	
$S_2A_1W_1$	-2.31 ^a		-12.77		-12.59 ^a	
$S_2A_1W_2$	-1.21 ^a		-11.00		-11.52 ^a	
$S_2A_1W_3$	-2.04 ^a		-9.69		-12.04 ^a	
S_2A_2			-8.75		-15.65	
$S_2A_2W_1$	-1.96		-8.37		-16.83	
$S_2A_2W_2$	-1.19		-8.35		-15.49	
$S_2A_2W_3$	0.60		-5.71		-14.42	
S_2A_3			-4.19			
S_3A_1			-16.14		-7.08	
S_3A_2			-13.84		-12.17	
S_3A_3			-8.93		-16.92	
S_3A_4			-7.42			
S_4A_1			-15.74		-4.16	
S_4A_2			-17.16		-7.48	
S_4A_3			-13.79		-12.34	
S_4A_4			-11.34		-16.26	
S_4A_5			-7.63			

951 ^a Nadykto and Yu, 2007; ^b Torpo et al., 2007; ^c Ortega et al., 2012; ^d Chon et al., 2007; ^e Kurten et al.,

952 2015.

953

954 **Table 4.** Same as Table 2 except for negatively charged clusters.

955

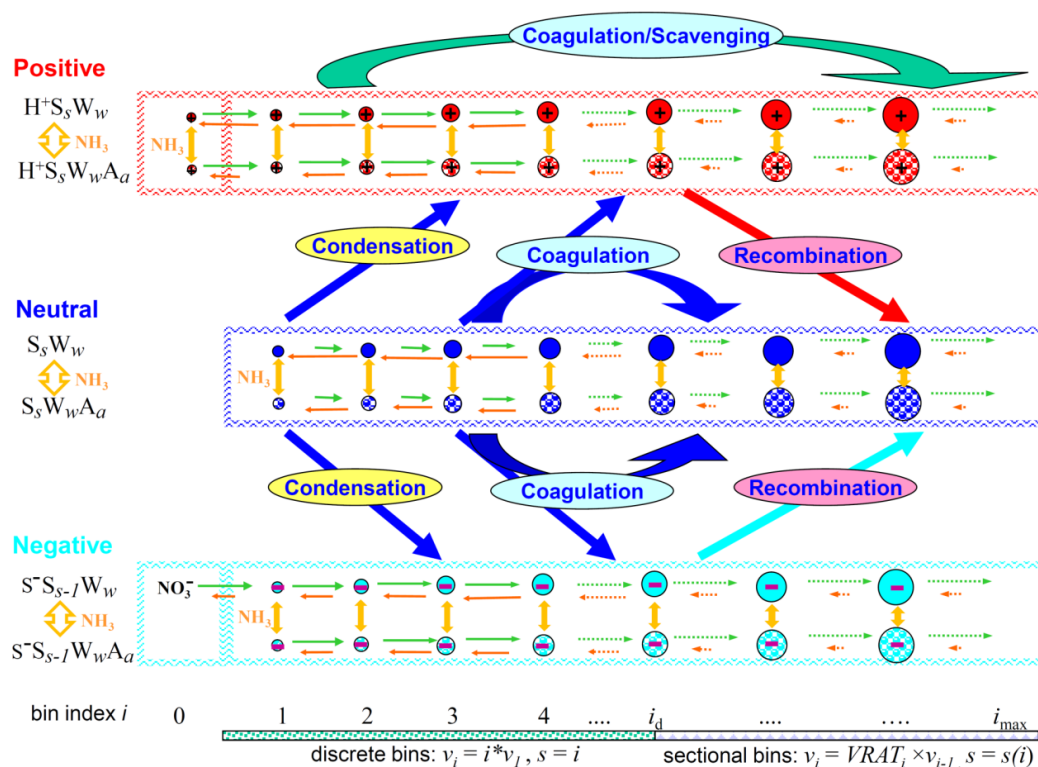
	ΔG_{+W}°		ΔG_{+A}°		ΔG_{+S}°	
	QC	experimental	QC	experimental	QC	experimental
$S^- A_1$			2.81			
$S^- S_1 W_0$					-32.74	-29.10 ^a
$S^- S_1 W_1$	-0.61				-28.12	
$S^- S_1 W_2$	-1.06				-25.36	
$S^- S_1 A_1$			0.08		-35.47	
$S^- S_2 W_0$					-15.06	-17.14 ^a
$S^- S_2 W_1$	-1.83				-16.28	
$S^- S_2 A_1$			-4.85		-19.99	
$S^- S_3 W_0$					-10.58	-13.28 ^a
$S^- S_3 W_1$	-2.92	-2.73 ^a			-11.67	-14.29 ^a
$S^- S_3 W_2$	-2.03	-1.53 ^a			-11.12	-13.80 ^a
$S^- S_3 W_3$	-2.01	-1.93 ^a			-11.52	-14.72 ^a
$S^- S_3 W_4$	-1.73					
$S^- S_3 A_1 W_0$			-11.89		-17.62	
$S^- S_3 A_1 W_1$	0.52		-8.45		-14.90	
$S^- S_3 A_1 W_2$	0.39		-6.03		-13.06	
$S^- S_3 A_2$			-7.27		-18.36	
$S^- S_3 A_3$			-4.66			
$S^- S_4 W_0$					-8.28	-10.96 ^a
$S^- S_4 W_1$	-3.50	-2.61 ^a			-8.86	-10.71 ^a
$S^- S_4 W_2$	-3.17	-2.79 ^a			-9.99	-12.10 ^a
$S^- S_4 W_3$	-2.65	-2.41 ^a			-10.64	-12.48 ^a
$S^- S_4 W_4$	-2.25	-2.14 ^a			-11.16	-12.77 ^a
$S^- S_4 A_1 W_0$			-15.37		-11.76	
$S^- S_4 A_1 W_1$	-2.21		-14.09		-14.49	
$S^- S_4 A_1 W_2$	-0.74		-11.66		-15.62	
$S^- S_4 A_2$			-12.23		-16.71	
$S^- S_4 A_3$			-7.59		-19.65	
$S^- S_4 A_4$			-6.72			

956 ^a Froyd and Lovejoy, 2003.

957



958



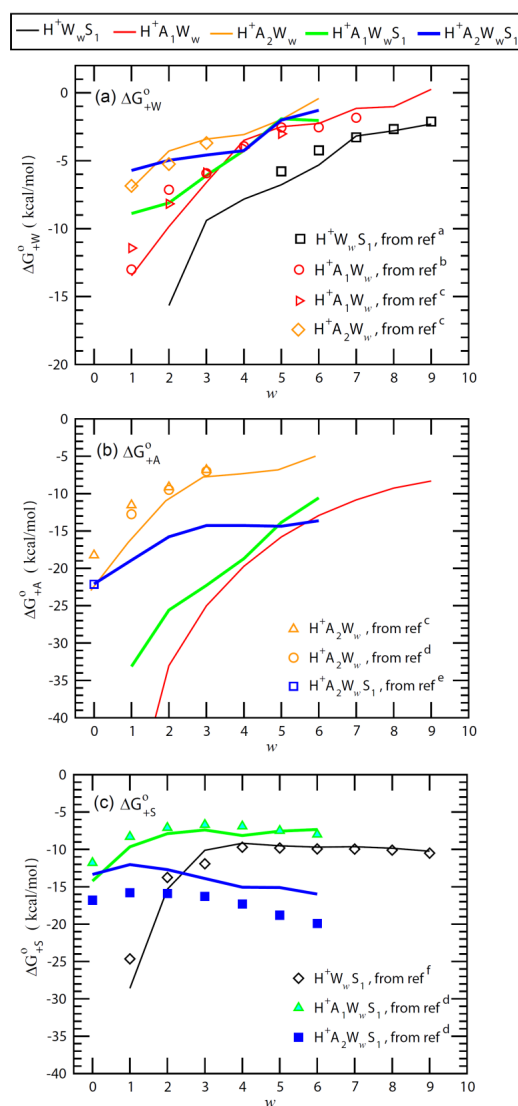
959

960

961 **Figure 1.** Schematic illustration of kinetic processes controlling the evolution of positively
 962 charged ($H^+S_sW_wA_a$), neutral ($S_sW_wA_a$), and negatively charged ($S^-S_{s-1}W_wA_a$)
 963 clusters/droplets that are explicitly simulated in the ternary ion-mediated nucleation (TIMN)
 964 model. Here S, W, and A represent sulfuric acid (H_2SO_4), water (H_2O), and ammonia (NH_3)
 965 respectively, while s , w , and a refer to the number of S, W, and A molecules in the clusters/droplets,
 966 respectively. The TIMN model has been extended from an earlier version treating binary IMN
 967 (BIMN) by adding NH_3 into the nucleation system and using a discrete-sectional bin structure to
 968 represent the sizes of clusters/particles starting from a single molecule up to background particles
 969 larger than a few micrometers.

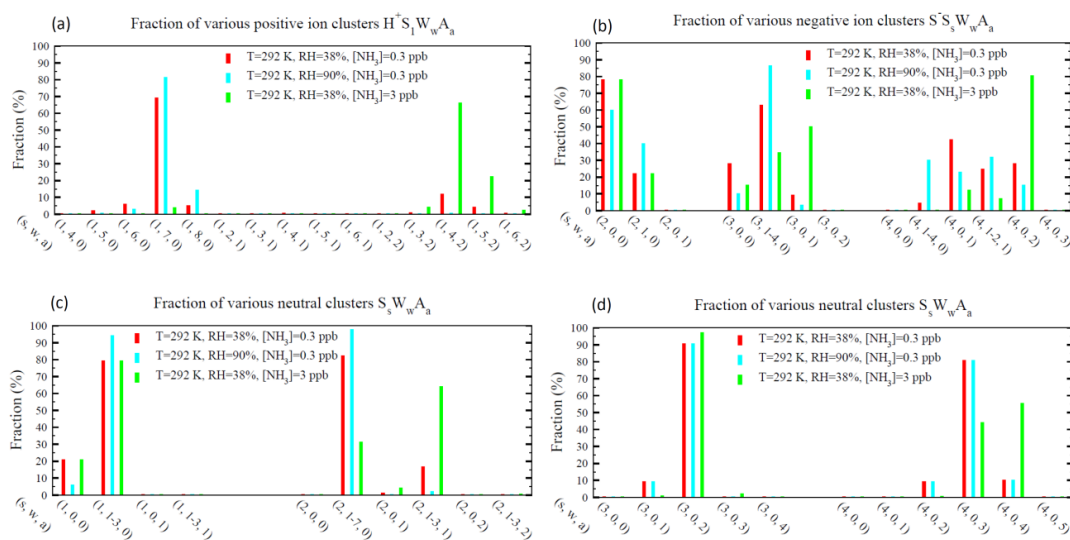


970



971

972 **Figure 2.** Stepwise Gibbs free energy change under standard conditions for the addition of a water
973 (ΔG_{+W}°), ammonia (ΔG_{+A}°), or sulfuric acid (ΔG_{+S}°) molecule to form the given positively charged
974 clusters as a function of the number of water molecules in the clusters (w). Lines are QC-based
975 values, and symbols are experimental results or semi-experimental estimates (see notes under
976 Table 2 for the references).



977

978

979 **Figure 3.** Relative abundance (or molar fraction) of small clusters containing a given number of

980 H₂SO₄ molecules for positive, negative, and neutral cluster types at a temperature of 292 K and

981 three different combinations of RHs (38% and 90%) and [NH₃] (0.3 and 3 ppb).

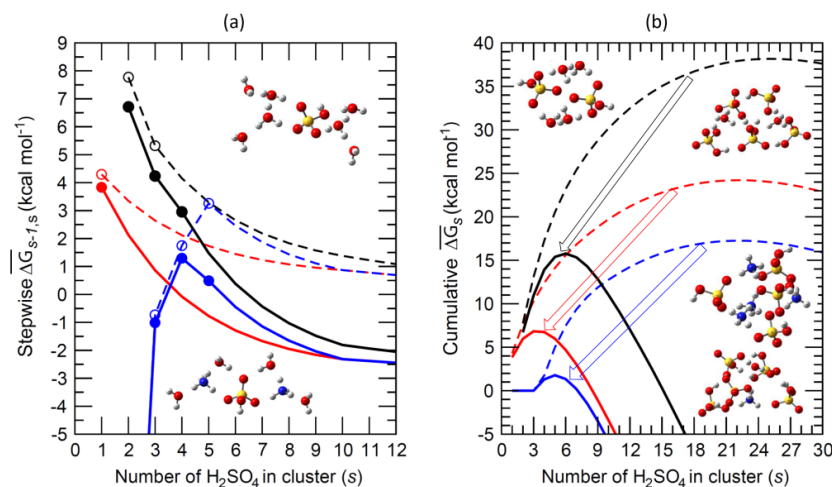
982

983

984

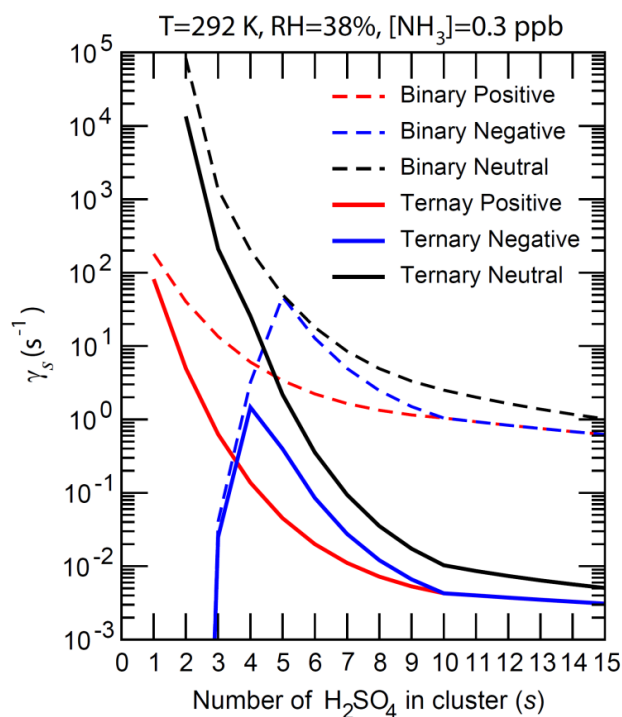


985



986
 987

988 **Figure 4.** (a) Average stepwise Gibbs free energy change for the addition of one H₂SO₄ molecule
 989 to form a neutral (black), positively charged (red), or negatively charged (blue) binary H₂SO₄-H₂O
 990 (dashed lines or empty circles) or ternary H₂SO₄-H₂O-NH₃ (solid lines or filled circles) cluster
 991 containing *s* H₂SO₄ molecules ($\overline{\Delta G}_{s-1,s}$); (b) Same as (a) but for the cumulative (total) Gibbs free
 992 energy change in each case. Filled and empty circles in (a) refer to $\overline{\Delta G}_{s-1,s}$ obtained using
 993 measurements and/or quantum-chemical calculations. $\overline{\Delta G}_{s-1,s}$ for larger clusters with $s \geq 10$, which
 994 approach the properties of the equivalent bulk liquid (20), are calculated using the capillarity
 995 approximation. Interpolation is used to calculate $\overline{\Delta G}_{s-1,s}$ for clusters up to $s=10$ (Eq. 11).
 996 Calculations were carried out at T=292 K, RH=38%, [H₂SO₄]=3×10⁸ cm⁻³ and [NH₃]= 0.3 ppb.
 997 The inset diagrams represent equilibrium geometries for the most stable isomers of selected binary
 998 clusters ((H₃O⁺)(H₂SO₄)(H₂O)₆, (H₂SO₄)₂(H₂O)₄, and (HSO₄⁻)(H₂SO₄)₄(H₂O)₂), and ternary
 999 clusters ((NH₄⁺)(H₂SO₄)(NH₃)(H₂O)₄, (HSO₄⁻)(H₂SO₄)₄(H₂O)(NH₃), (H₂SO₄)₄(NH₃)₄).



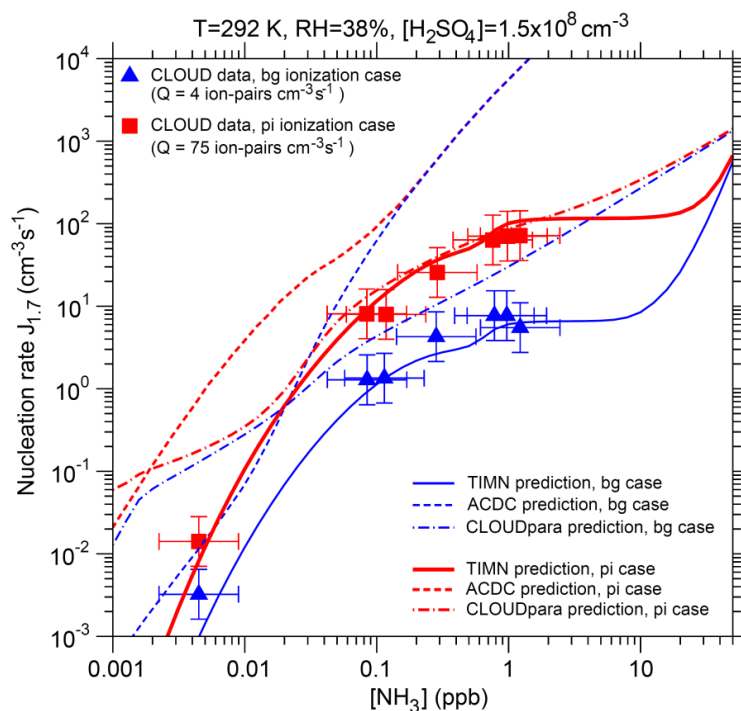
1000

1001 **Figure 5.** The number-concentration-weighted mean evaporation rates ($\bar{\gamma}$) of H_2SO_4 molecules
1002 from neutral clusters (black), positively charged clusters (red), and negatively charged clusters
1003 (blue) for binary ($\text{H}_2\text{SO}_4\text{-H}_2\text{O}$, dashed lines) and ternary ($\text{H}_2\text{SO}_4\text{-H}_2\text{O-NH}_3$, solid lines) nucleating
1004 systems containing s H_2SO_4 molecules ($\overline{\Delta G_{s-1,s}}$). $T=292$ K, $\text{RH}=38\%$, and $[\text{NH}_3] = 0.3$ ppb for
1005 the ternary system.

1006

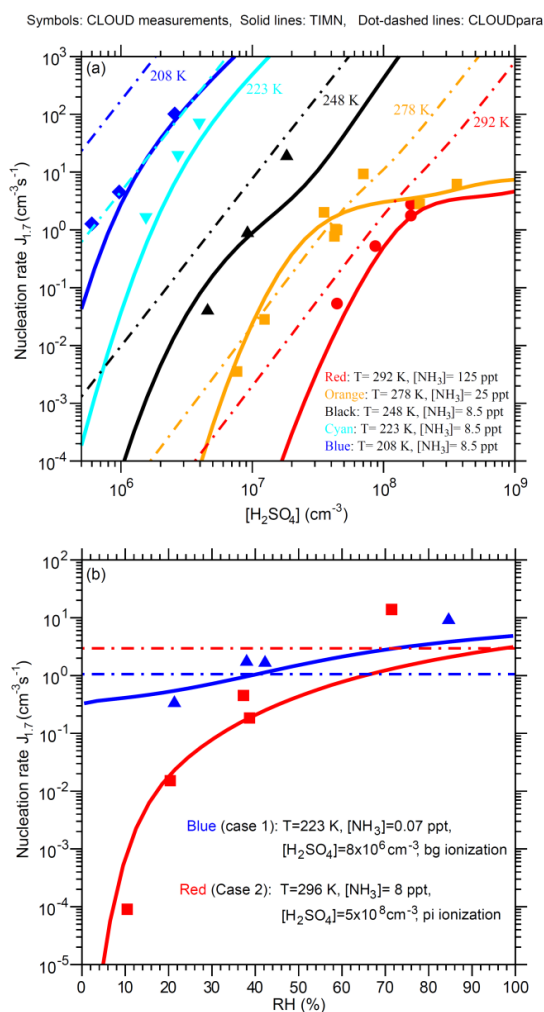
1007

1008



1009

1010 **Figure 6.** Effect of ammonia concentrations ($[\text{NH}_3]$) on effective nucleation rates calculated at a
1011 cluster mobility diameter of 1.7 nm ($J_{1,7}$, lines) under the stated conditions with two ionization
1012 rates (Q) – background ionization, bg (blue), and ionization enhanced by a pion beam, pi (red).
1013 Also shown are predictions from the TIMN model, the Atmospheric Cluster Dynamics Code
1014 (ACDC) (McGrath et al., 2012; Kurten et al., 2016), and an empirical parameterization of CLOUD
1015 measurements (CLOUDpara) (Dunne et al., 2016) are indicated by solid, dashed, and dot-dashed
1016 lines, respectively. The symbols refer to CLOUD experimental data (Kirkby et al., 2011; Dunne
1017 et al., 2016), with the uncertainties in measured $[\text{NH}_3]$ and $J_{1,7}$ shown by horizontal and vertical
1018 bars, respectively. To be comparable, the CLOUD data points given in Dunne et al. (2016) under
1019 the conditions of $T=292$ K and $\text{RH}=38\%$ with $[\text{H}_2\text{SO}_4]$ close to $1.5 \times 10^8 \text{ cm}^{-3}$ have been
1020 interpolated to the same $[\text{H}_2\text{SO}_4]$ value ($=1.5 \times 10^8 \text{ cm}^{-3}$).



1021

1022 **Figure 7.** Comparison of TIMN simulations (solid lines), CLOUDpara predictions (Dunne et al.,
 1023 2016) (dot-dashed lines) and CLOUD measurements (symbols, data from Dunne et al. (2016) of
 1024 the dependences of nucleation rates on (a) $[\text{H}_2\text{SO}_4]$ at five different temperatures ($T=292$, 278,
 1025 248, 223, and 208 K) and (b) RH at two sets of conditions as specified. $[\text{NH}_3]$ is in ppt (parts per
 1026 trillion, by volume). Error bars for the uncertainties in measured $[\text{H}_2\text{SO}_4]$ (-50%, +100%), $[\text{NH}_3]$
 1027 (-50%, +100%), and $J_{1,7}$ (overall a factor of two) are not shown. To be comparable, the CLOUD
 1028 data points given in Dunne et al. (2016) under the conditions (T, RH, ionization rate) with $[\text{NH}_3]$
 1029 or $[\text{H}_2\text{SO}_4]$ close to the corresponding values specified in the figure legends have been interpolated
 1030 to the same $[\text{NH}_3]$ (Fig. 7a) or $[\text{H}_2\text{SO}_4]$ (Fig. 7b) values.

1031